Computers and Geotechnics 164 (2023) 105799

Contents lists available at ScienceDirect

Computers and Geotechnics

journal homepage: www.elsevier.com/locate/compgeo

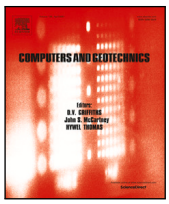

Research paper

Surface layer method for analysis of slope stability using finite elements

Tomáš Kadlíček *, David Mašín

Faculty of Science, Charles University, Albertov 6, 128 00 Praha 2, Czech Republic

ARTICLE INFO

Keywords:
Elastoplasticity
Mohr–Coulomb
Slope stability
Strength reduction method
Surface layer

ABSTRACT

This paper introduces a surface layer method for the analysis of slope stability using finite elements. When stability of a slope is calculated using the strength reduction method, the slope typically fails at local surface irregularities, which leads to numerical divergence that stops the calculation. It is then impossible to quantify the factor of safety for potentially dangerous landslides of larger dimensions. In this paper, a method is introduced in which a weightless elastic surface layer is applied at the surface, which aims to stabilize the surface of a numerical model during the strength reduction. A vertical cut through the surface layer then predefines the surface contour of the landslide, while the shape and depth of the slip surface along with the associated factor of safety is the output of the analysis. A typical use-case scenario is when the landslide shape is known *a-priori* (for example when analysing existing landslides). If it is not known, various landslide shapes can be tested by searching for an outline with the lowest factor of safety. This is similar to the limit equilibrium method, where a complete slip surface including its surface trace must be predefined. The proposed method was validated using parametric studies both in 2D and 3D; its importance is most pronounced in 3D where the surface morphology is highly complex. Practical application of this method is demonstrated by the back analysis of the Dobkovičky landslide, which occurred in 2013 during construction of the highway D8 in Czech Republic.

1. Introduction

Evaluation of a slope stability is one of the most thoroughly discussed topics in geotechnics. On the practical side, the topics discussed vary from preliminary evaluation of hazardous areas to unique structure designs or back calculations of disastrous failures. The theoretical side is often focused not only on the development of new methods but also on analysing and testing seemingly proven approaches.

In this article, various geometrical and material conditions of the affected area are analysed in the pursue for the identification of the most probable cause of the Dobkovičky landslide. To thoroughly examine the cause of the landslide, 3D numerical model was developed with yearly LIDAR measurement and site investigation. Due to the high degree of geometrical complexity, the regular application of the Strength Reduction Method (SRM) would not provide relevant results. To select a proper method for the investigation, a comprehensive summary of the currently available stability analyses theories and approaches were reviewed which resulted in the application of the weightless elastic surface layer during the SRM analysis. This method stabilizes the surface of the numerical model and prevents insignificant local failures. Before its application in the case study, properties and behaviour of the elastic surface layer was tested on selected geometries of slopes.

2. Methods of slope stability analyses

The Limit Equilibrium Method (LEM), sometimes called the slices method (Bishop, 1954), is based on the idea of dividing a soil mass above the examined slip surface into a number of slices (Taylor, 1937). Slicing a soil body yields the problem statically indeterminate, which requires a certain level of assumption regarding the interslices acting forces (Krahn, 2011). Although the method is based on pure statics without considering a displacement, a number of the established methods such the Bishop (1954), simplified (Janbu, 1954) and Petterson (1955) methods do not satisfy both the force and momentum equilibrium (Duncan, 1996). Methods which satisfy all equilibrium conditions simultaneously, such as Morgenstern and Price (1965), Spencer (1967), Janbu (1973) and Sarma (1979), are referred to as rigorous methods (Duncan, 1996). The factor of safety (*FS*) is in general determined from the ratio of resisting and acting forces on a given slip surface. The fact that the *FS* corresponds to a single predetermined slip surface necessitates an iterative (Chen et al., 2011; Zhou and Cheng, 2013) or statistical (Xie et al., 2003) procedure to find the most critical one. The results are often conveniently displayed in the form of a rotational centres grid with related *FS*s. Localization of the minimum

* Corresponding author.
E-mail address: tomas.kadlicek@natur.cuni.cz (T. Kadlíček).

https://doi.org/10.1016/j.compgeo.2023.105799
Received 26 April 2023; Received in revised form 7 September 2023; Accepted 11 September 2023
Available online 26 September 2023

FS can be accompanied by iterative difficulties since the minimum *FS* is in the rotational centres grid surrounded by locations with non-converging areas (Krahn, 2011). The issue related to stress evaluation was significantly improved with the so called Enhanced Limit Strength Method (ELSM) (Fredlund et al., 1999; Chugh, 2003; Krahn, 2011; Stianson et al., 2011, 2015; Liu et al., 2015), which takes advantage of the stress analysis performed in the Finite Element Method (FEM). Extensions of the original LEMs, such as those of Bishop (Hungr, 2015; Zhang et al., 2017), Janbu (Huang et al., 2002), Spencer (Chen et al., 2011) and Morgenstern–Price (Zheng, 2012), to a three dimensional (3D) space divides a soil body above a slip surface to columns. To be considered as the rigorous method, LEMs in 3D have to satisfy six equilibrium conditions (Duncan, 1996) and, although fully rigorous methods were developed (Zheng, 2012; Zhou and Cheng, 2013), not all methods upheld this requirement (Hungr, 2015; Huang and Tsai, 2000). The 3D extensions are based on the original assumptions of the intercolumns forces and require iterative processes or have to find the most critical *FS*. Simplicity of LEMs enables efficient analyses of large hazardous areas (Carrara et al., 1991) when linked with a Geographic Information System (GIS) (Xie et al., 2003, 2006a,b; Jia et al., 2012).

Another prevalent approach to stability analyses is the Limit Analysis Method (LAM). This method is based on the principle of virtual work and thus two forms of LAM are distinguished, an upper and lower bound. While the upper bound LAM (Sloan, 1989; Lyamin and Sloan, 2002b; Chen et al., 2005), the kinematic approach, stems from the principle of virtual displacement, the lower bound (Sloan, 1988; Lyamin and Sloan, 2002a; Camargo et al., 2016), or static approach, originates from the principle of virtual forces. In principle, the actual *FS* is bracketed within the lower and upper bounds (Li et al., 2009). LAM is divided in two groups, analytical (Michalowski and Drescher, 2009; Michalowski and Nadukuru, 2013; Wang et al., 2019a; Yang and Wei, 2021) and numerical (Bottero et al., 1980; Lyamin and Sloan, 2002b,a; Chen et al., 2005; Li et al., 2009). While the analytical approach focuses on a direct calculation of the *FS*, the numerical LAM is embedded in numerical methods such as FEM to determine the stress distribution in a soil body. Linking the numerical LAM with the adaptive meshing showed excellent results (Borges et al., 2001; Lyamin et al., 2005; Tschuchnigg et al., 2015a). The analytical LAMs *a-priori* define the shape of the slip surface, which can be developed from a composited 3D slip surface (Ugai, 1985; Leshchinsky and Baker, 1986; Gens et al., 1988) or a single surface defined by an ellipsoid or horn-like shape (Michalowski and Drescher, 2009; Wang et al., 2019b). The analytical approach is thus restricted to problems with simple geometries (Chen et al., 2005).

The Strength Reduction Method (SRM) (Zienkiewicz et al., 1975; Matsui and San, 1992) in FEM is founded on an incremental reduction of the soil strength until the limit equilibrium of internal and external energy is reached. The actual *FS* is then calculated as a ratio of the initial and reduced strength parameters at the moment of equilibrium. Although SRM is mostly applied for the Mohr–Coulomb (MC) failure criterion, it was also developed for more advanced constitutive models such as barodesy (Schneider-Muntau et al., 2018) and hypoplasticity (Kadlíček and Mašín, 2020). These methods take advantage of the evaluation of the *FS* based on the mobilized strength in the slip surface as proposed in Nitzsche and Herle (2020); however, more thorough testing is needed in this regard. The key feature of SRM is that the most critical slip surface is localized naturally without any preconcieved assumptions and visualized with the increased accumulation of shear strains along the slip surface. Nonetheless, only one slip surface can be localized during SRM. Unlike LEM or analytical LAM, there is no need for an *a-priori* assumption regarding the position or shape of a slip surface (Griffiths and Marquez, 2007; Nian et al., 2012). In addition, SRM can simulate a progressive failure of a structure and, thanks to the nature of FEM, it also enables sequential construction and analysis of a given case (Griffiths and Marquez, 2007). Furthermore, LAM considers only the associated flow rule of the MC model, i.e., the direction of the plastic strain increment given by the dilatancy angle ψ is identical to the friction angle φ ($\psi = \varphi$) (Šejnoha, 2015). The associated flow rule provides a higher estimate of the *FS* than the non-associated flow rule and thus furnishes a non-conservative estimate of the *FS* (Manzari and Nour, 2000; Tschuchnigg et al., 2015a,c; Chen et al., 2020; Lin et al., 2020), and more importantly, the non-associated flow rule better corresponds to the behaviour of a soil. Therefore, the non-associated flow rule is usually preferred in geotechnical plastic analyses. Nevertheless, studies on the effect of the selected flow rule show serious numerical issues when using the non-associated flow rule ($\psi \neq \varphi$) (Tschuchnigg et al., 2015a). The problem stems from the instability of the MC model on the level of a constitutive equation if the non-associated flow rule is considered, which can generate a negative work density along proportional loading paths (Rudnicki and Rice, 1975; Maier and Hueckel, 1979). The 2D study of the flow rule performed by Tschuchnigg (Tschuchnigg et al., 2015a,b) and Chen (Chen et al., 2020) showed that the instability can be treated with the so called Davis approach (Davis, 1968), which modifies both ψ and φ to obey the associated flow rule. Although the Davis approach reportedly improved the numerical issues in 2D, a later study in 3D (Lin et al., 2020) did not show the anticipated improvement. The SRM method is often associated with FEM, however, this method was also applied in the numerical manifold method (NMM) in 2D by Yang et al. (2023) and 3D (Yang et al., 2021, 2022) analyses, which naturally enables simulation of both continuous and discontinuous geotechnical problems and thus represents a convenient alternative to FEM.

Although the dependency of Young's modulus E was not found to affect the resulting *FS*, Poisson's ratio ν showed some influence on the *FS*. The 2D analysis in Zheng et al. (2005) called this issue "$\varphi - \nu$" inequality. The effect of ν was also observed for LAM (Stianson et al., 2015). It should also be mentioned that the *FS* determined using numerical approaches are inherently dependent on factors such as the iterative method used, step size, permitted error value, maximal number of iterations and the FEM mesh distribution and fineness (Cheng et al., 2007; Tschuchnigg et al., 2015a,c). The later issue can be greatly improved with adaptive meshing (Peraire et al., 1987; Zienkiewicz et al., 1995; Borges et al., 2001; Lyamin et al., 2005).

Three common criteria are used in SRM to determine the slope failure (Tu et al., 2016). First, a common numerical criterion is the loss of convergence. The idea is that the strength of the soil is reduced until the point when a new balance of internal and external energy cannot be reached and thus the limit energy state is found. Second, the *FS* is determined based on a displacement analysis of a representative node: The *FS* is selected as the moment when the displacement experiences a sudden change in magnitude (Griffiths and Lane, 1999). Third, more intuitive option is to determine the *FS* from the points when the shear band is clearly propagated though the soil body (Matsui and San, 1992). The study in Tu et al. (2016) proposed new criteria based on energy interchange during SRM, which was in agreement with the aforementioned criteria; however, more specific classifications were provided. In this paper, the first two criteria are used to determine the *FS*.

Although SRM is a well established method, relevant studies and improvements are still undertaken and issues related to this method are far from simple. The growth of computational power has enabled an increasing scale and deeper level of detail in numerical models, which has resulted in more prevalent use of 3D FEM. It is well established that 2D analysis provides a conservative *FS* when compared with 3D analysis for the same geometry and setting (Ugai, 1985; Chugh, 2003; Griffiths and Marquez, 2007). However, 3D analysis is invaluable when dealing with a higher degree of complexity or when the third dimension gains on importance (Griffiths and Marquez, 2007). In some cases, when the surface of the numerical model is rough, the main advantage of SRM, i.e., the naturally localized slip surface with the lowest *FS,* can become its disadvantage because the slip surface propagates either through the surface layers of the numerical model or in an area that

is not relevant to the problem under consideration. Consequently, the level of model complexity has to be simplified, often significantly, to the detriment of obtaining results. While the simplification can be relatively easy in the case of 2D geometry, it can be a difficult task when dealing with 3D geometry. Valuable comparisons of the methods mentioned can be found in Duncan (1996), Griffiths and Lane (1999), Wei et al. (2009), Krahn (2011) and Nian et al. (2012).

In this paper, a simple approach to 2D and 3D SRM is proposed that enables evaluation of the *FS* even for complicated 3D geometries. The method consists of application of a weightless elastic the surface layer, which stabilizes surface of the numerical model and thus prevents evaluation of the *FS* based on local failures, which are irrelevant for the overall stability of a slope. The surface layer is then interrupted to induce the desired surface contour of the slope failure. The usefulness of the method is demonstrated using back-analysis of the slope failure of the Dobkovičky landslide, which occurred in 2013 during the construction of the highway D8 in the Czech Republic. The method is simple and can be applied in any finite element code that supports a strength reduction method without further modifications. All the analyses presented in this paper were performed in Plaxis 3D.

The strength reduction method is used in the paper, which is based on the reduction of the strength parameters φ and c of the MC model. Once the strength reduction method starts, the reduction factor *MSF* is gradually increased and the reduced values of the friction angle and cohesion are calculated by

$$\tan\varphi_{red} = \frac{\tan\varphi}{MSF} \tag{1}$$

and

$$c_{red} = \frac{c}{MSF} \tag{2}$$

In each increment, the energy of internal and external forces is balanced out while producing additional deformations. The factor MSF is increased until equilibrium cannot be achieved. The reached *MSF* then represents the factor of safety, *FS*, of the slope. In the Plaxis implementation, the dilatancy angle ψ remains constant until the equality $\varphi = \psi$ occurs. Then the dilatancy ψ starts decreasing with φ since $\psi > \varphi$ is not allowed for. The terminating criteria of SRM used in this paper are the default ones in Plaxis 3D.

3. Surface layer method adopted in analyses of a slope with a simple artificial geometry

A simple geometry is created to test the effects of the surface layer when subjected to SRM. As a benchmark, the numerical model is allowed to naturally collapse; selected failure mechanisms are then induced with a help of the surface layer method. Keeping in mind the highlighted issues of SRM, the parametric study focuses on the effects of the parameters of the surface layer (Young's modulus E and Poissons's ratio ν) and on the surface layer geometry (layer thickness and cut width).

3.1. Configurations of the numerical models

The first geometry is a 3D equivalent of the 2D plane strain model. It is a simple homogeneous gentle slope inclined at 20° to horizontal. The finite element mesh used is displayed in Fig. 1.

For the study purposes, a small bulge was placed approximately in the middle on the slope, as shown in Fig. 2. The bulge was a sub-slope inclined 49°, which imitated surface irregularity at the slope surface. Therefore, SRM should be able to identify failure of the bulge, with a lower factor of safety than the *FS* of the overall general slope. The surface layer was applied over the surface of the numerical model, and two parallel vertical "cuts" were introduced onto the surface layer, which would drive the collapse of the slope between these two openings. The surface layer was 20 m high and the cuts were 5 m wide; these values varies in later parametric studies.

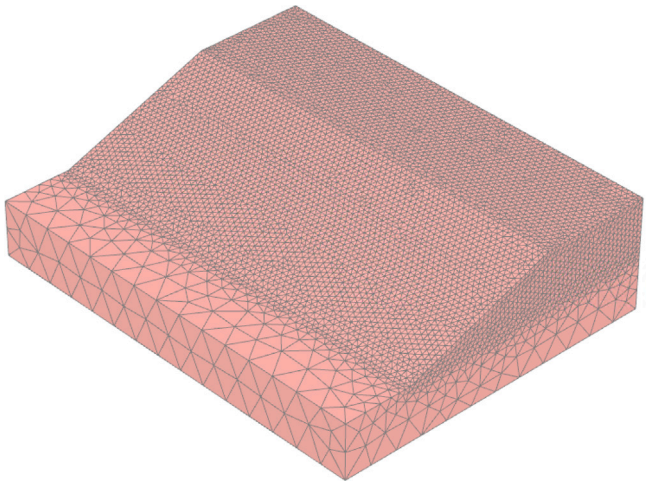

Fig. 1. FEM mesh of the homogeneous slope.

Table 1
The generic parameters used in the parametric study.

Constitutive model	φ [°]	c [kPa]	ψ [°]	E [MPa]	ν [–]	γ [kN/m^3]
Mohr–Coulomb	30.0	10.0	0.0	20.0	0.3	19.0
Elasticity	0.0	0.0	0.0	20e3	0.3	0.0

The slope body (yellow) and its base (brown) was characterized using the MC model as having five parameters φ (friction angle), c (cohesion), ψ (dilatancy angle), E (Young's modulus) and ν (Poisson's ratio). The values adopted for the model parameters are summarised in Table 1. The surface layer must be weightless with $\gamma = 0$ kN/m^3, since its application should not change the stress state inside of the slope.

3.2. Collapse without the surface layer

Two cases of slope collapses without the surface layer were simulated first as a reference point. In the first case, the bulge was present on the slope, while in the second case the slope was homogeneous. The analysis with the bulge determined that the *FS* was 1.917 and without the bulge 2.142. The final distribution of shear strains γ_s at the end of SRMs are displayed in Fig. 3. It should be noted that, additionally to the fact that the bulge changes the failure mode from the whole slope to the bulge only, it also has a minor effect on stability even if the shear zone is not affected through its mass. An additional analysis was thus run with an elastic bulge of the same weight, leading to the *FS* of 2.114.

3.3. Application of the surface layer method

In the following sections, the elastic surface layer is used as a supporting tool during the strength reduction analysis. The recommended order of computational phases and application of the elastic surface layer is as follow:

(1) Calculation of the geo-static stress
(2) Intermediate construction phases
(3) Application of the elastic surface layer in the full extent
(4) Performing a vertical cut in the elastic surface layer outlining the landslide
(5) Strength reduction analysis

Note that if the vertical cuts are applied instantly, that is the points 3 and 4 are unified, the phase calculation is less stable but the resulting FS is the same.

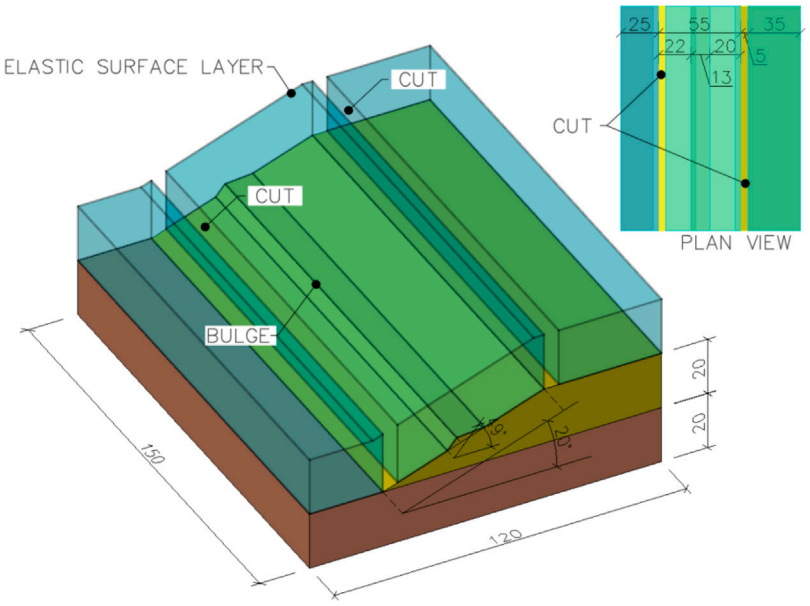

Fig. 2. The adopted geometry of the homogeneous slope with elastic surface layer.

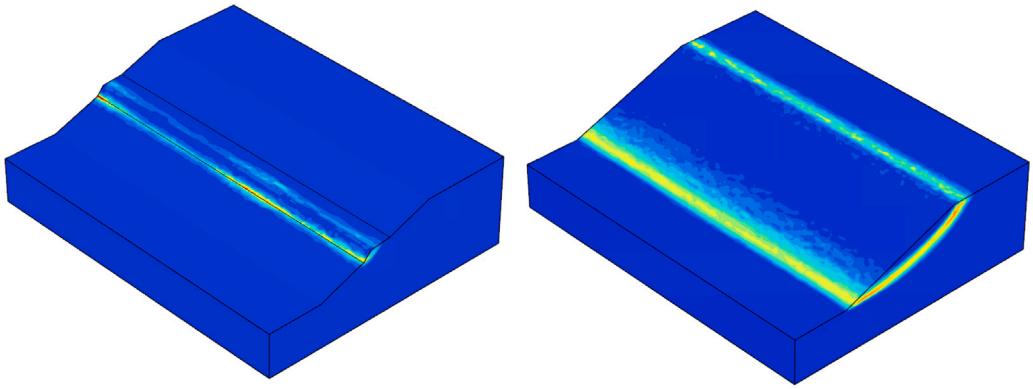

(a) Collapse of the bulge (b) Collapse of the homogeneous slope

Fig. 3. Isolines of shear stains γ_s for the two cases of collapse calculated without a surface layer.

3.3.1. *Effect of surface layer elastic parameters*

The first study focused on the effect of the Young's modulus E of the surface layer. The results of the analyses are displayed in Fig. 4, which shows the dependency of the *FS* on the ratio of the Young's modulus of the surface layer E_S and the Young's modulus of the slope material E_{MC}. This figure shows that for small values of the surface layer stiffness (E_S/E_{MC} = 0.00001), the results are equivalent to the simulations without a surface layer since it is that soft and does not have a stabilising effect. With increasing E_S/E_{MC}, the *FS* increases, converging towards stability of a slope without a bulge for $E_S/E_{MC} \geq$ 0.1. Additional analyses were conducted for E_{MC} = 30 MPa and E_{MC} = 100 MPa, while the E_S was increased accordingly so that the ratios E_S/E_{MC} from Fig. 4 were the same. These analyses resulted in the same outcome as shown in Fig. 4, which implies that the ratio of the corresponding stiffnesses plays a crucial role.

The development of *FS*s during SRMs analyses from Fig. 4 is shown in Fig. 5. It can be observed that for the ratios $E_S/E_{MC} \geq 0.1$, the factor of safety stabilises during the iteration process to the final value, while for lower values of E_S/E_{MC} the FS evolves gradually.

Accumulation of the shear strains γ_s for the case E_S/E_{MC}=1000 is shown in Fig. 6(a). Propagation of the slip surface through the slope body is clearly visible. Although shear strains γ_s can be observed on the surface of the bulge caused by slipping of the surface layer on the

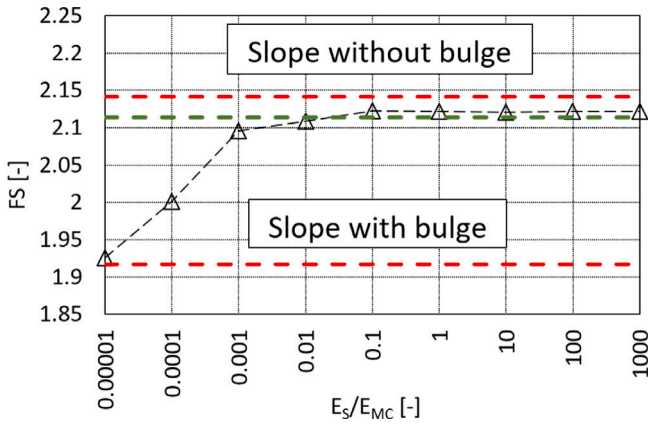

Fig. 4. Development of *FS* with E_S/E_{MC} ratio. The upper limit defines the slope stability without the bulge. The lower limit defines the stability of the bulge. For the sake of clarity, the slope stability with the elastic bulge is displayed with the green colour.

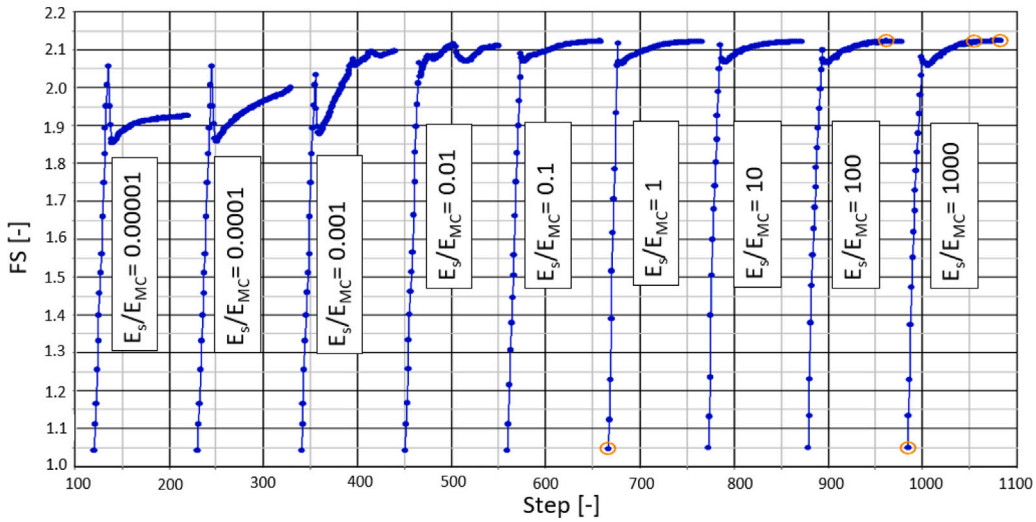

Fig. 5. Evolution of *FS*s from the parametric study on Young's modulus E.

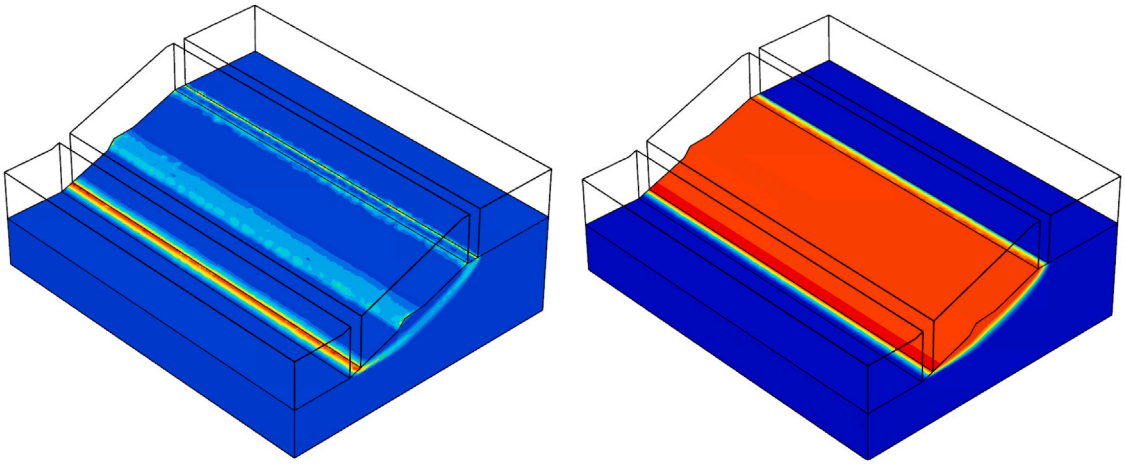

(a) Isolines of shear strains γ_s (b) Isolines of displacements u

Fig. 6. Analysis at the end of SRM with the elastic surface layer for the stiffness ratio EC/E_{MC}=1000.

bulge surface, their values are small. The isolines of displacement in Fig. 6(b) show a uniform distribution and thus a homogeneous slope failure.

The propagation of the slip surface through the slope body of the stiffness ratios from $E_S/E_{MC} = 1000$ to $E_S/E_{MC} = 0.01$ follow the same path as shown in Fig. 6(a) and differ only in the magnitude of displayed shear strains γ_s. The ratios $E_S/E_{MC} = 0.0001$ and 0.00001 exhibit the same failure mechanism as displayed in Fig. 3a for the failure of the bulge alone. The transition between these two modes of failure is displayed in Fig. 7 with the ratio $E_S/E_{MC} = 0.001$, recall Fig. 5.

When there is a sufficiently high stiffness of the surface layer ($E_S/E_{MC} \geq 0.1$), the surface of a numerical model stabilizes and prevents local failures as a solver iteratively distributes displacements to locations of lower stiffness. The parametric study was also performed for Poisson's ratio ν, but was not found to have any effect on the calculated factor of safety.

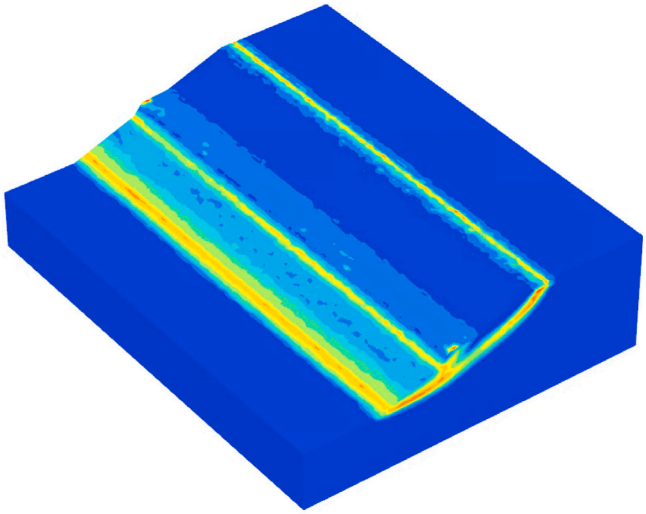

Fig. 7. Transitional mode for failure for the stiffness ratio $EC/E_{MC} = 0.001$.

3.3.2. *Effect of surface layer height*

By default, the height of the elastic surface layer used in the analyses was 20 m. Different heights of 3, 5, 10, 15 and 20 m were also tested to evaluate the effect of height on the *FS*, see Fig. 8. It should be noted that the height of the surface layer is referred to the height above

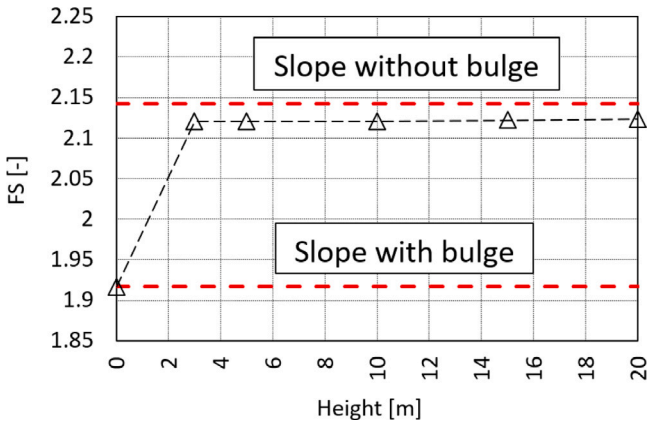

Fig. 8. Development of *FS* with the height of the elastic surface layer.

the homogeneous slope, however, the depth of the surface layer in a location of the bulge was measured as 2.5 m and 0.6 m in the of case 5 m and 3 m height, respectively. The results showed that the height of the surface layer did not influence the calculated *FS* in any case. This implies that the key attribute to be considered in the surface layer method is the tangent stiffness of the soil element and its degradation during SRM rather than the bending stiffness of the surface layer.

3.3.3. Effect of cut width in the surface layer

The effect of the cut width through the surface layer was tested next. The width varied from 2.5 m to 22.5 m, while the default width used in the analyses was 5 m. These two limit cases are displayed in Fig. 9a. The dependence of *FS* on the cut width is shown in Fig. 9b. It shows that the width of the cut did not influence the *FS* as long as the cut did not encroach into the bulge.

3.3.4. 2D comparative analyses

A comparative analysis to the homogeneous 3D slope was performed in 2D. The slope had the same cross section as its 3D counterpart. The 2D FEM mesh was generated using 6-noded quadratic elements (Fig. 10) which are equivalent to 10-noded quadratic elements used in Plaxis 3D. Three SRM analyses were performed to evaluate the stability of the bulge, the slope without the bulge and the stability with the elastic surface layer.

In 2D, a clear propagation of the slip surface from the top to the bottom of the slope through the openings in the elastic layer can be observed with some slippage of the surface layer on the bulge surface unaffecting the homogeneous failure mode (Fig. 11). The elastic surface layer thus has an analogous effect in the 2D and 3D analysis.

Regarding factors of safety, the 2D analyses resulted in lower values for the *FS* than the 3D analyses. Stabilities for the natural collapse were calculated as $FS = 2.061$ ($FS = 2.142$ in 3D) and $FS = 1.770$ ($FS = 1.917$ in 3D) for the simple slope and for the slope with a bulge, and $FS = 2.059$ ($FS = 2.122$ in 3D) for stability with the surface layer. The difference between factors of safety calculated in 3D and 2D analyses, which should in principle be equivalent, can be, however, attributed to the mesh density effects. Significant refinement of 3D mesh (counting 1.13 million finite elements) results in the factors of safety $FS = 2.074$, $FS = 1.797$ and $FS = 2.058$ in the case of the simple slope, bulge and analysis with the elastic surface layer, respectively, which is close to $FS = 2.061$, $FS = 1.770$ and $FS = 2.059$ calculated in 2D.

3.3.5. Investigation of small surface irregularities

For this analysis, the geometry was modified so that the bulge covered only a small portion the slope as seen in Fig. 12; the plane strain analogy was thus cannot be applied any more. The geometry was tested with the default setting and different values of Young's modulus for the surface layer, see Fig. 13. The evolution of the *FS* with different Young's modulus shows results similar to these seen in Fig. 4, however, the stabilization has a more pronounced effect since a $FS = 2.141$ is reached in almost all cases except for the ratio $E_S/E_{MC} = 1e{-}5$. Recall that the stability of the homogeneous slope was achieved when the $FS = 2.143$. The stability of the slope with the surface layer was thus closer to the stability of the homogeneous slope because the smaller bulge under the elastic surface layer had less mass, which itself affects stability to a small extent. It should be stressed that in this case, the stability of the bulge was determined as FS=1.704. This case thus shows that small surface irregularities can be efficiently stabilized using the surface layer method. It should be pointed out that the term *"surface irregularities"* is rather subjective. Here, we refer to a geometrical spatial variabilities resulting from global measurements such as Lidar or photogrammetry. These measurements often produce dense clouds of surface measurements with many irregularities which stop calculation of a standard SRM in FEM, while having a negligible effect on the factor of safety of deeper major slip surfaces. Surface layer method aims at overcoming this problem, filtering out the effect of minor surface irregularities which enables to calculate factor of safety of the major failure zone.

3.3.6. Limited slope failure width

This case aims to determine the limitations of the surface layer method when only a section of the slope is selected to fail. The same geometry as for the homogeneous slope was used; however, the cut in the surface layer was modified according to Fig. 14.

The *FS* of the limited homogeneous slope and the limited bulge failures were calculated as $FS = 2.254$ and $FS = 1.941$, respectively. These values were slightly higher than in the case of a complete failure due to the stabilizing effect of the 3D model, described also by Ugai (1985), Chugh (2003), Griffiths and Marquez (2007). Since a short section of the bulge can be exposed in the cut, it can significantly affect the resulting *FS* and thus a study of the cut width was undertaken; these results are summarized in Fig. 15, for cut widths of between 1 m and 10 m.

The results show that the cut width has a noticeable impact on the *FS*. The width of 1 m corresponds to one element being positioned in the cut. This element is connected to both parts of the elastic surface layer and thus it deforms based on the movement of the inner part of the elastic surface layer. As the cut widens, more elements are located between both sides of the cut and thus they can be subjected to the effect of SRM with local bulge failure inside the cut. This is demonstrated in Fig. 16, which shows a homogeneous failure of the slope in the case of a cut width of 1 m and a significant displacement concentration of the bulge when the cut width is 10 m.

3.3.7. Position of the vertical cut

The presented method is suitable in cases when the surface outline of the landslide is known *a-priori*. In the cases when the position is not known, the most critical outline of the landslide must be searched iteratively. Nonetheless, the method searches automatically for the slip surface shape below the ground, which makes it significantly different to LEM where many slip surfaces must be tested for a given entry and exit positions (in 2D) or surface contours (in 3D). Different positions of the vertical cut will lead to different FSs. This is demonstrated in Fig. 17, where the individual FSs increases with increasing distance of the vertical cut from the slope edge. Recall that the most critical slip surface in found naturally at the distance 0 m from the slope edge with $FS = 2.122$, recall Fig. 6.

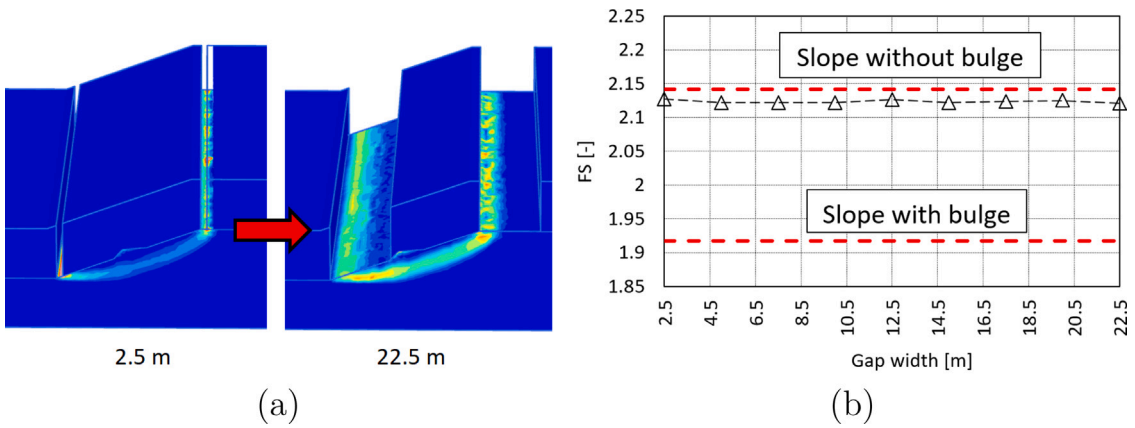

Fig. 9. Development of *FS* with the width. Slope geometry and developed shear strains γ_s (a) and the depenedency of FS on the cut width (b).

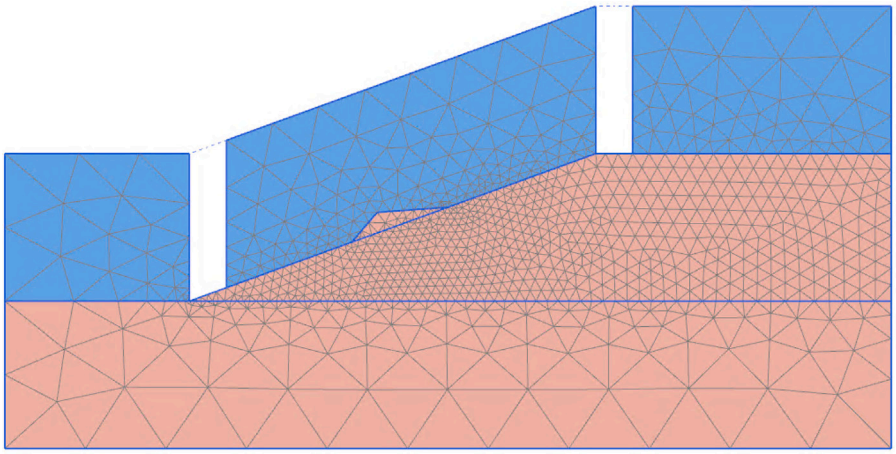

Fig. 10. Geometry of 2D numerical model.

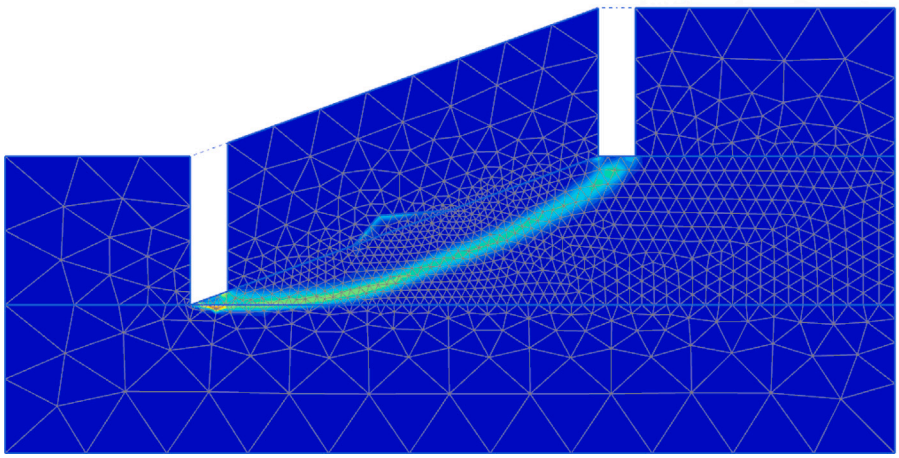

Fig. 11. Isolines of shear strains γ_s in 2D analysis.

3.3.8. 3D corner and valley slope geometries

Practical problems usually involve irregular slope geometries. To further test the surface layer method, two additional geometries were created, denoted as corner and valley, see Fig. 18. Both geometries have the same inclination of 20° as the homogeneous slope. In each case, the vertical cut in the elastic surface layer predefined a failure mechanism of the slope along a small ellipsoidal area which differed from the one provided by the classical approach. Furthermore, the cut in the surface layer was set to 1 m wide, which corresponded to the size of one element.

Firstly, both geometries were subjected to SRM without application of the surface layer method (see Fig. 19). The calculated factor of safety was $FS = 2.166$ and $FS = 2.18$ for the corner and valley models, respectively. As expected, the failure of both geometries was located outside

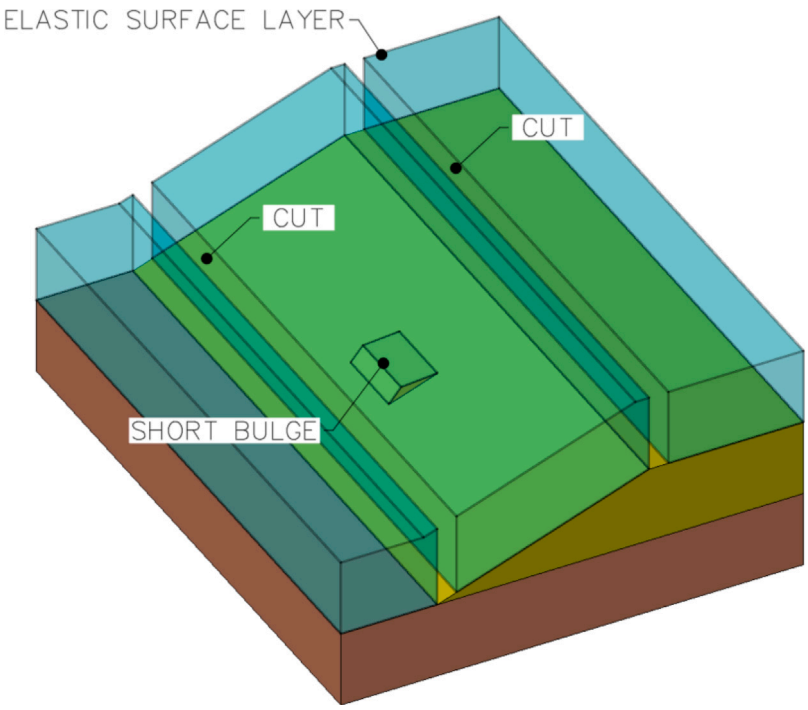

Fig. 12. Geometry of the numerical model with a small bulge.

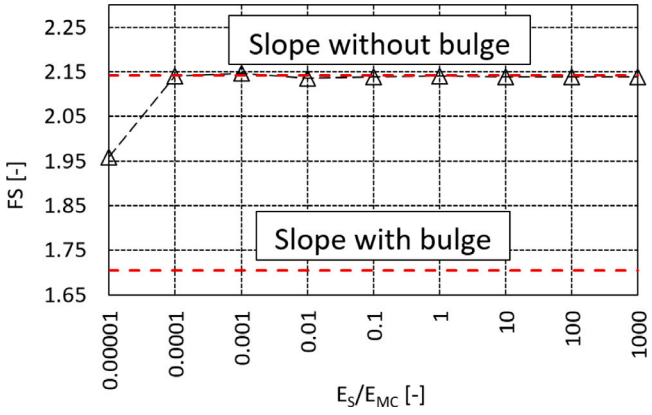

Fig. 13. Development of *FS* with E_S/E_{MC} ratio for the geometry with the small bulge.

of the respective corner or valley as they are of lower inclination and thus higher stability.

Thereafter, the first ellipsoidal cuts were positioned in close proximity to these more stabilized zones. Isolines of displacements $|u|$ in Fig. 20(a) indicate a homogeneous failure. The cross section from Fig. 20(a) shows propagation of the slip surface through the slope corner as predefined by the cut (Fig. 20(b)). The stability was evaluated as $FS = 3.379$.

The results of the predefined failure in the case of the valley geometry is displayed in Fig. 21. In this case, the slip surface was very shallow with gradual deepening as loading from the sides of the valley increased with the distance from the top, see Fig. 21(b). The obtained stability was $FS = 3.399$.

The results presented in Figs. 20–21 show that the failure mechanisms outlined on distinct 3D geometries in Fig. 18 were correctly determined by the applied elastic surface layer.

3.4. Discussion of the surface layer method validation

The surface layer method has two key purposes: Firstly, to stabilize the surface of a rough numerical model in order to prevent the failure of small surface irregularities. Secondly, to cause a preferential location of the slope to fail. Although this is an often mentioned shortcoming of the LEM methods, it can become an advantageous approach if an outline of a landslide is known *a-priori* (such as in the case of an existing older landslide, see Section 4) and the use of SRM alone would cause a failure of an irrelevant area. In addition, it is to be emphasized that the LEM and SRM approach with surface layer are not identical regarding the search for the most critical slip surface. While, in the LEM, many slip surfaces must be tested considering the failure surface position and shape below the ground, in SRM with surface layer the entry and exit points only (in 2D) or surface contours (in 3D) must be predefined. The method then automatically searches for the most critical shape of the slip surface below the ground. When this is not the case, the method is used in a manner similar to the limit equilibrium method, which tests a large number of slip surfaces by searching for the slip surface with a minimal *FS* value. When using the surface layer method, though, only the surface contour of the slip surface must be specified in an iterative manner, while depth and shape of the slip surface is controlled by the finite element model itself. The parametric analyses using artificial examples in this section revealed the following findings:

1. The resulting *FS* was only dependent on the Young's modulus E of the elastic surface layer as long as it was very low, with the ratio E_S/E_{MC} below 0.1. The ratio $1 < E_S/E_{MC} < 10$ is recommended in real case analyses to efficiently stabilise the surface while not introducing large stiffness gradients into the model.
2. The height of the applied surface layer was found not to have any effect on the resulting *FS* as long as it was sufficiently high to stabilise all irregularities.
3. The width of the cut in the surface layer significantly influenced the resulting *FS*. If the width is large enough to accommodate small surface irregularities consisting of several elements, the mesh fails locally. The width of the cut thus should be limited to

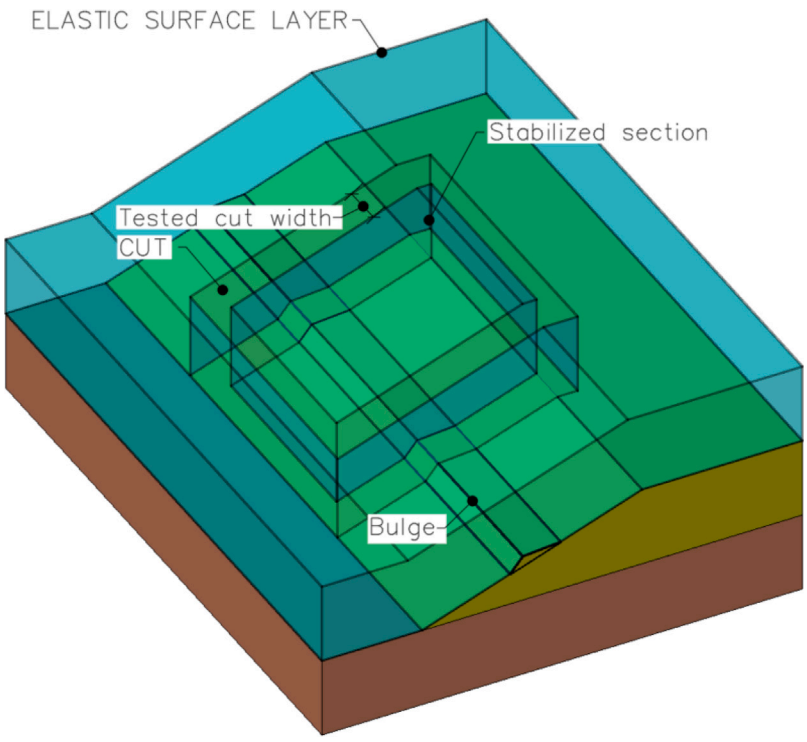

Fig. 14. Geometry of the numerical model with small bulge.

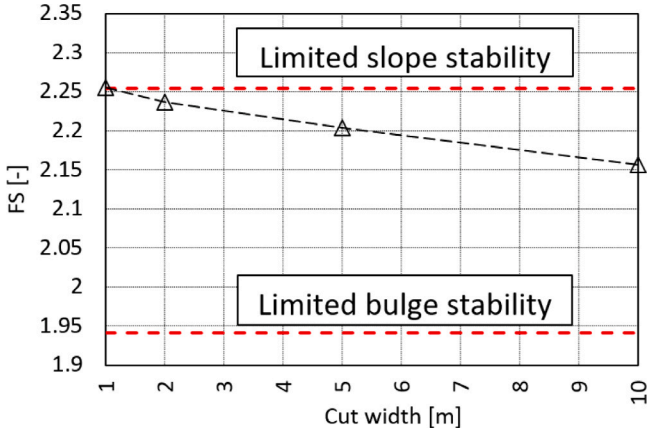

Fig. 15. Influence of the cut width on the resulting *FS*.

the size of few (typically one or two) finite elements to eliminate shear band evolution inside the cut. When this is the case, the cut width does not influence significantly the calculated factors of safety. The shape of the FEM mesh in the cut has to be inspect visually to assure this recommendation.

4. Demonstration of the surface layer method for predictions of stability of a real landslide

In this section, the surface layer method is applied in the practical case of the Dobkovičky landslide. The failure occurred in 2013 during the construction phase of the highway D8 between Prague (Czech Republic) and Dresden (Germany), passing through the Central Bohemian Uplands (Fig. 22). The study aimed to determine a probable cause of this landslide. The analysis was described in detail in the court investigation reports by Stemberk et al. (2016, 2019).

The area geologically consists of Cretaceous marlstones, which were covered by horizontally deposited Mesozoic magmatic flows (basalts) and occasionally by pockets of pyroclastic material (tuffs), see geological cross-section in Fig. 23. While the overall inclination of the slope is relatively small (approximately 9°), the top part of the slope is steeper as it is stabilised by the layer of volcanic material. The Cretateous marlstones are prone to the development of residual strength with a friction angle of approx. 14°. The slope in its upper part is supplied by groundwater from the permeable basalt rocks, which, in combination with low residual strength, leads to unstable conditions. The landslides were well documented in the area by geotechnical surveys conducted since 1972. As is clear from Fig. 22, there is a basalt quarry located in the top part of the slope, while the highway cut was located in the bottom part; there is also a single-track railway line situated between the quarry and the highway. Loading of the top part of the slope by the quarry dump, combined with a highway cut in the bottom section combined with a supply of groundwater from basalt rocks infiltrating through the quarry bottom during the rainy period of May to June 2013 constituted an obviously unfavourable condition leading to the slope failure. The slope failed on June 7th 2013 at a maximum rate of approx. 3 m per hour. The slip surface was located at a shallow depth of between 4 to 6 meter below ground surface, and was approx. 200 m wide and 500 m long with an estimated total mass of 455,000 m^3. The 3D finite element model, created as a part of the court investigation report by Stemberk et al. (2016) and presented here, aimed to quantify the effect of individual factors contributing to the slope failure (quarry dump, highway cut, railway line).

In the numerical model, the area was divided into quasi-homogeneous sections (see Fig. 23) of similar geologic position and mechanical material parameters, which were found during pre-failure and post-failure geotechnical site investigations. The parameters are summarised in Table 2.

The surface geometry of the model was taken from the LIDAR data collected in 2012 and thus before the actual slope failure. The geometry of geological layers was based on a significant amount of real boreholes (55 in total), supplemented by additional artificial boreholes meant to create a smoother and continuous shape of the underground layers, see

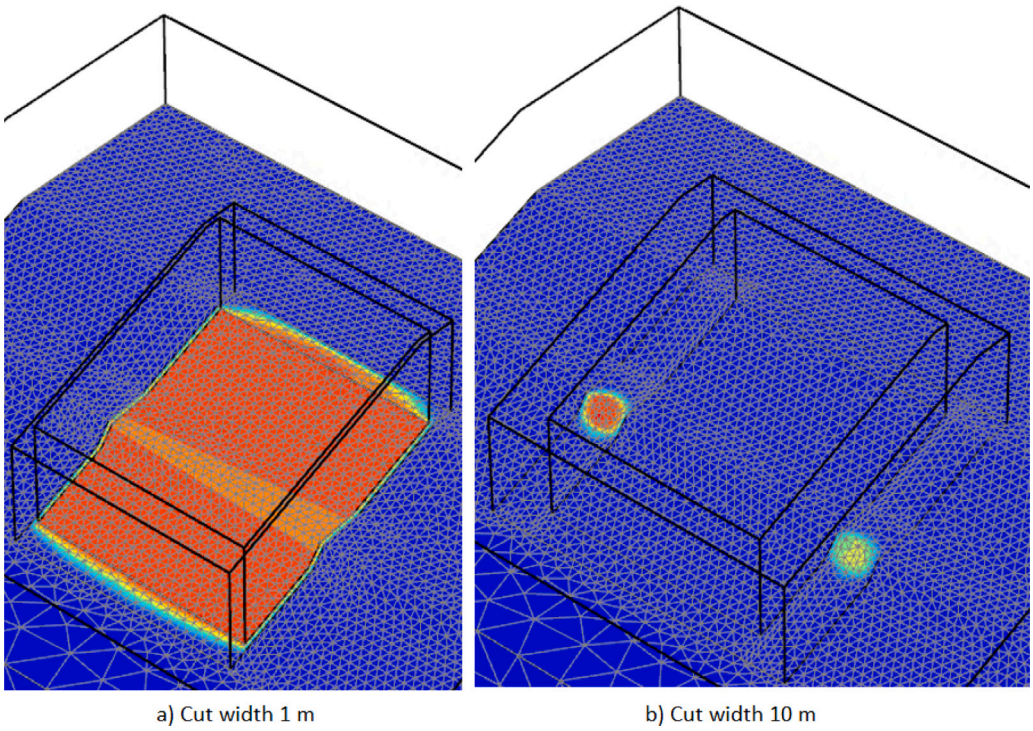

Fig. 16. Isolines of displacement |u| for different cut widths.

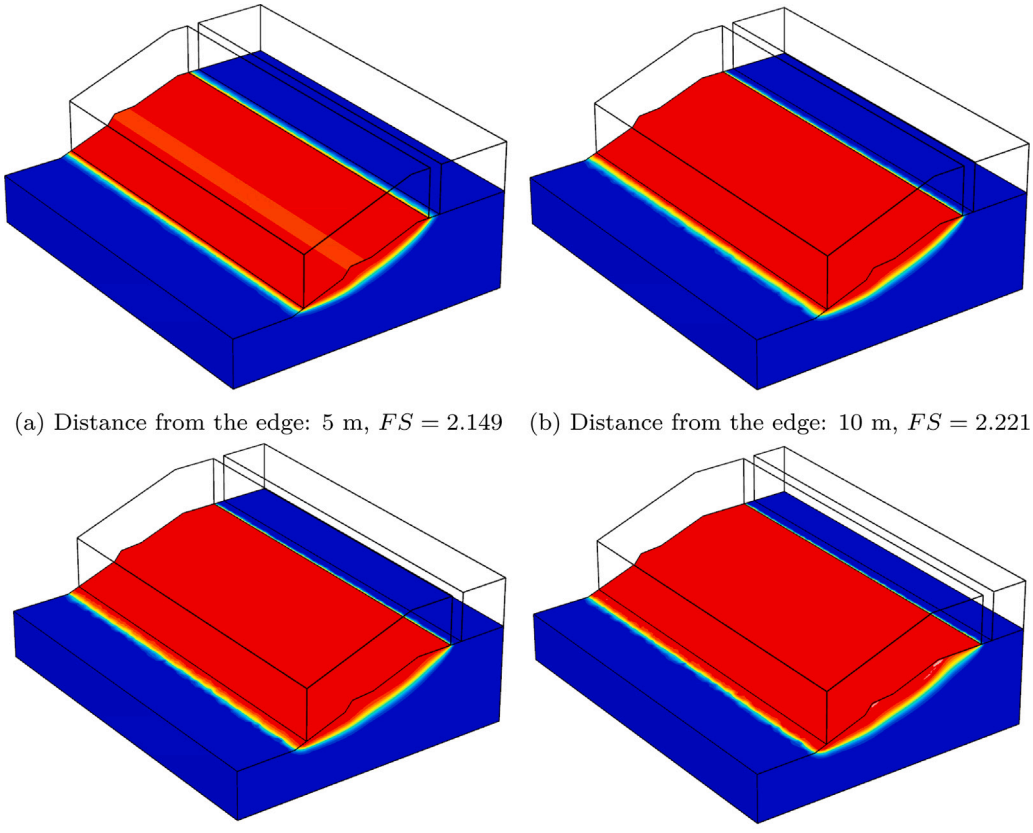

Fig. 17. Total displacements $|u|$ after the SRM analysis. Various positions of the vertical cut and its impact on the resulting FS.

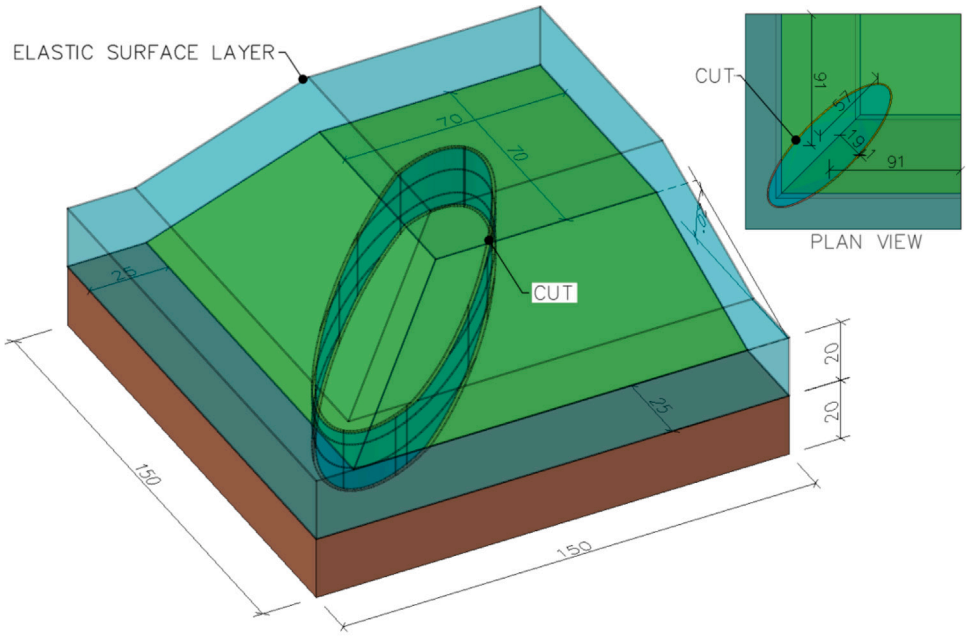

(a) Corner

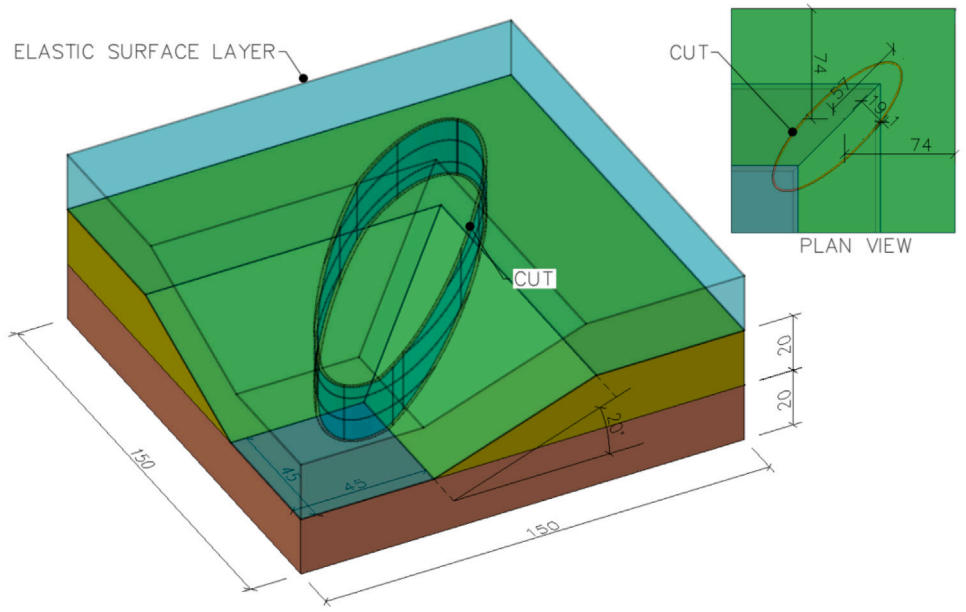

(b) Valley

Fig. 18. The corner and valley geometries of the numerical model with displayed predefined failure mechanisms.

Fig. 24. The initial stress state was calculated by the means of gravity loading.

Since the goal of the analyses was to identify the effects of individual factors affecting the stability of the slope (quarry dump, highway cut, railway embankment), the analyses were repeated for four different geometries identified in Table 3 and in Fig. 25. In each case, the numerical model covers an area of 440 × 420 m. Geometry NG I (actual slope before failure) is directly taken from LIDAR surface data obtained in 2012, while the shape of the quarry dump was modelled in GIS software based on available quarry dump photos taken just before the landslide. In geometry NG IV, the quarry dump and quarry operation-related rockfill material on the steep slope below the quarry floor were removed by supplementing the top part of the slope by LIDAR data from 2015, taken after loose rockfill removal during landslide stabilisation. For geometry NG III, the railway embankment was manually removed from the model using GIS software. In geometry NG II, the lower portion of the slope was supplemented by LIDAR measurements from 2009, which were taken before highway cut was built.

Two extra steps between the plastic *in-situ* stress analysis and strength reduction were included to apply the surface layer method. In the first additional step, an elastic weightless surface layer of height of 20 m was placed into the model to cover the surface (Fig. 26a). In the second additional step, a 6 m wide cut was created in the surface layer which followed the contour of the real Dobkovičky landslide (Fig. 26b). The strength reduction method was applied next. Due to application of the surface layer method, the simulation did not search for a slide of the lowest factor of safety as normal, but it searched for the lowest factor of safety of the landslide outlined by the surface

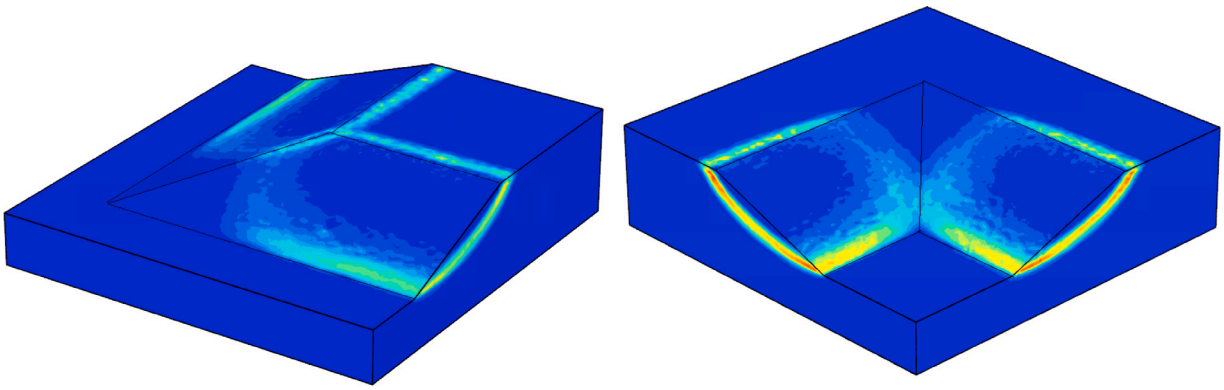

(a) Corner (b) Valley

Fig. 19. The slip surfaces highlighted with shear strains γ_s.

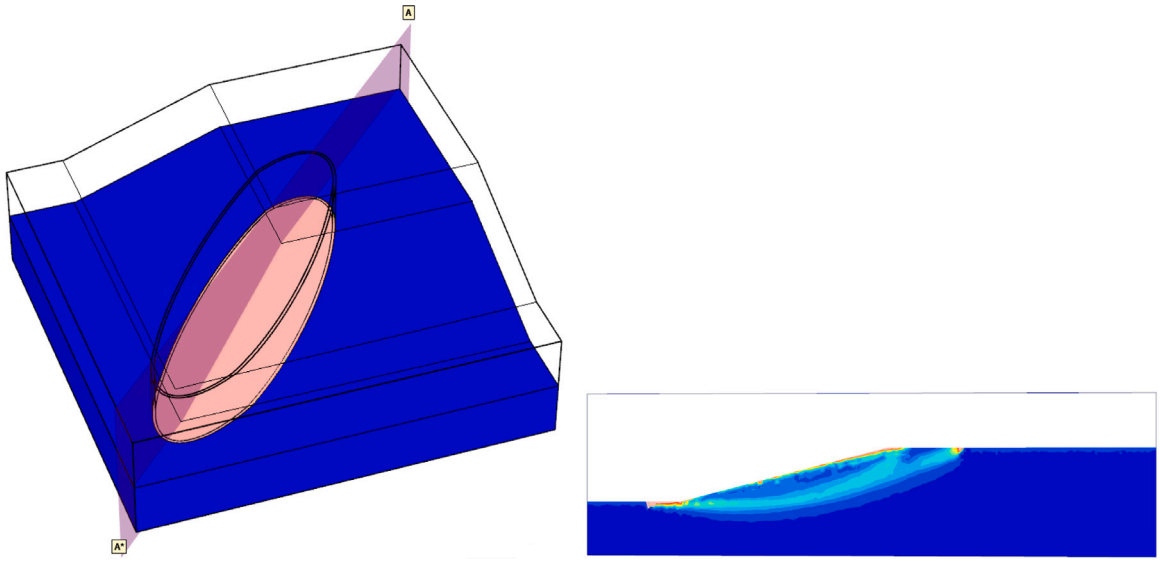

(a) Isolines of displacements $|u|$ (b) Isolines of shear strains γ_s

Fig. 20. Results of the corner stability analysis specified through surface layer cut.

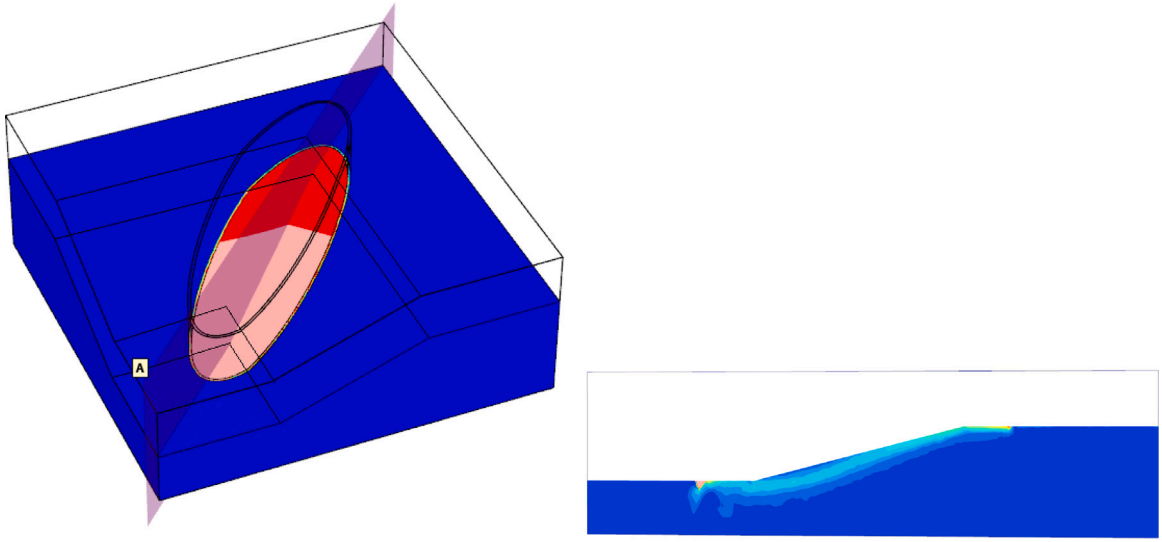

(a) Isolines of displacements $|u|$ (b) Isolines of shear strains γ_s

Fig. 21. Results of the valley stability analysis specified through surface layer cut.

Fig. 22. Aerial photo of the landslide and surrounding area two years after the Dobkovičky landslide occurred (source https://mapy.cz).

Table 2
Parameters of the Mohr–Coulomb model used in finite element simulations of the Dobkovičky landslide.

	φ_c [°]	c [kPa]	ψ [°]	E [MPa]	ν [–]	γ_{unsat} [kN/m^3]	γ_{sat} [kN/m^3]
Quaternary fine	25.4	0.0	0.0	20.0	0.3	21.0	12.5
Quaternary coarse	28.0	0.0	0.0	20.0	0.35	19.0	20.0
Basalt rockfill	34.0	0.0	0.0	20.0	0.31	19.0	20.0
Marlstone weathered	15.0	0.0	0.0	20.0	0.36	21.0	21.5
Tuff in shear zone	15.0	0.0	0.0	20.0	0.34	18.5	19.5
Tuff	29.0	0.0	0.0	20	0.34	18.5	19.5
Basalt fresh	–	–	–	200.0	0.10	23.0	23.5
Marlstone fresh	–	–	–	200.0	0.10	19.5	20.5

Table 3
Model geometries used in simulations.

Numerical geometry	Quarry deposit	Railway embankment	Highway cut
NG I	X	X	X
NG II		X	X
NG III	X		X
NG IV	X	X	

layer—it was, however, still free to select shape and depth of the slip surface. This is an important feature since the shape and depth on the slip surface was not known in detail, only its surface contour. It should be mentioned that application of the SRM without the elastic surface layer caused local failure in the area of the highway landfill and thus did not provided any information about relevant causes of the slope failure.

Prior to conducting the stability analyses, several studies were done to define the final model geometry and setup, such as testing the finite element mesh coarseness and the Young modulus of the elastic surface layer (see the artificial example above for more details). In total, six cases with differing geometries (see Fig. 25 and Table 3), groundwater level depths (groundwater level at failure, located 1–2 m below ground, and groundwater level corresponding to the base of Quaternary sediments representing groundwater in dry periods) and assumed strength parameters of the shear zone (critical state or residual) were generated as follows:

Table 4
Factors of safety for individual stability analyses at $|u| = 1$ m.

Simulated case	FS	FSn
Case A	1.227	1.000
Case B (without quarry deposits)	1.349	1.099
Case C (deep groundwater)	1.413	1.151
Case D (without railway)	1.200	0.978
Case E (without highway cut)	1.268	1.033
Case F (critical state parameters)	1.649	–

- A - Real slope geometry (NG I) and the groundwater level at the failure, residual strength parameters.
- B - Like A, but without Quarry deposits (geometry NG II).
- C - Like A, but with deep groundwater corresponding to dry periods.
- D - Like A, but without railway embankment (geometry NG III).
- E - Like A, but without highway cut (geometry NG IV).
- F - Like A, but with critical state strength parameters for the shear zone.

Although the rise of precipitation had a profound effect on the slope stability, the detected slip surface was located below the groundwater level before the failure occurred. It is therefore justified that the increased positive pore water pressure acting on the slip surface was modelled solely with the increased ground water level.

The relationship between the strength reduction factor MSF and the displacement $|u|$ at the surface in the centre of the landslide is shown in Fig. 27. It is clear that, for all curves, the reached values of MSF are higher than 1. This was, indeed, caused by various modelling uncertainties and imperfections, in particular the shear strength parameters, but also the uncertain positions of the geological layers, groundwater table, etc. As the factor of safety of Case A is known to be equal to 1, results of the simulations have first been normalised to the MSF from Case A as

$$MSF_n = \frac{MSF}{MSF_{case\ A}} \tag{3}$$

For the normalisation, a hyperbolic regression of Case A MSF evolution has been adopted as $MSF_{case\ A} = 1 + |u|/(1.2 + 3.2|u|)$ (regression curve is also shown in Fig. 27a). Normalised factors of safety for each scenario, FS_n, were then assumed to be equal to MSF_n for the individual cases at $|u| = 1$ m (this deliberately chosen value did not affect the results significantly as the MSF_n curves were for larger $|u|$ values stabilised). The final values of the calculated safety factors are shown in Table 4. Note that the FS_n was not calculated for Case F, because it was assumed that a significant source of the uncertainty was the strength parameters of the shear zone, and thus normalisation for critical state parameters through analysis based on residual parameters would be incorrect; uncertainties of the two strength types do not necessarily need to be correlated.

The failure mode is shown in Fig. 28; Case A and Case E (without highway cut) were selected as examples. For case A, it is clear that the landslide follows the predefined contours, with larger displacements in the upper part of the slope indicating a lower local factor of stability. It is interesting to observe from Fig. 28d that, for Case E, the landslide is actually shorter than defined by the cut in the surface layer; the bottom section of the approx. 70 m surface layer slips on the ground surface. The surface layer method was thus able to not only find the stability of a landslide with a predefined contour, as in the case A, but also a landslide shape smaller than defined by the surface layer cut outline. It should be noted that this was possible thanks to adoption of critical state parameters with zero cohesion for the top subsurface soil layers (Quaternary deposits), see Table 2.

The results of stability analyses can be summarized as follows:

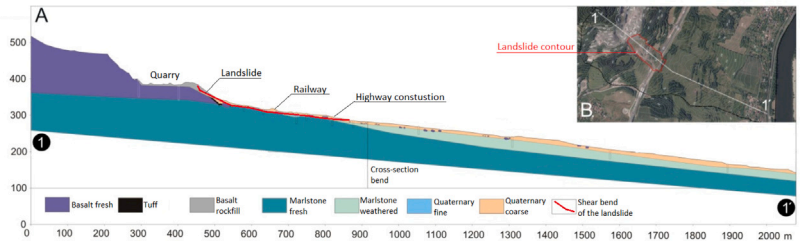

Fig. 23. Geological cross-section along the Dobkovičky landslide.

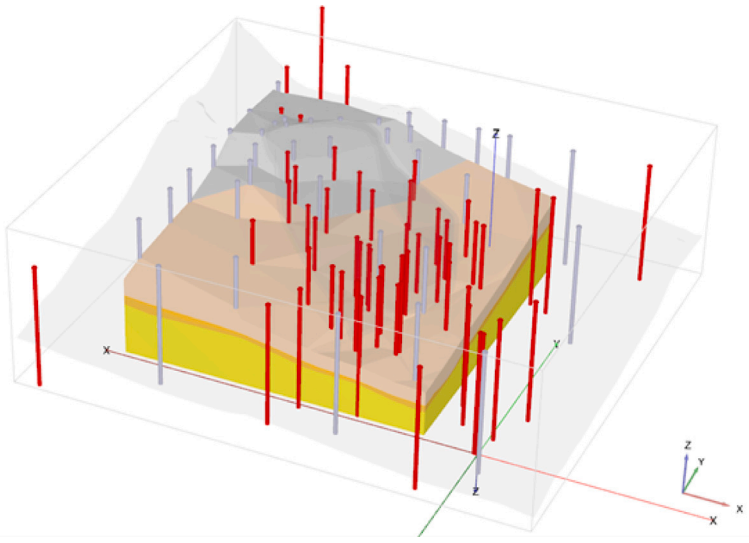

Fig. 24. Position of boreholes used for generation of the numerical model geometry. Real boreholes are shown in red, while artificial boreholes implemented to improve a geometry of the numerical model are depicted in grey.

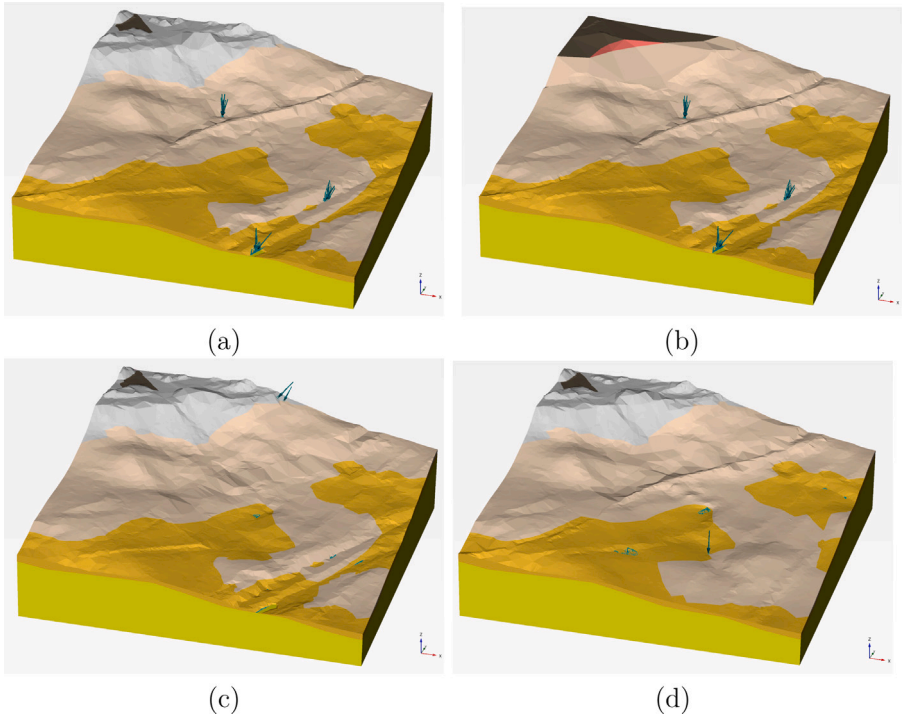

Fig. 25. Numerical model with complete geometries NG I (a) to NG IV (d).

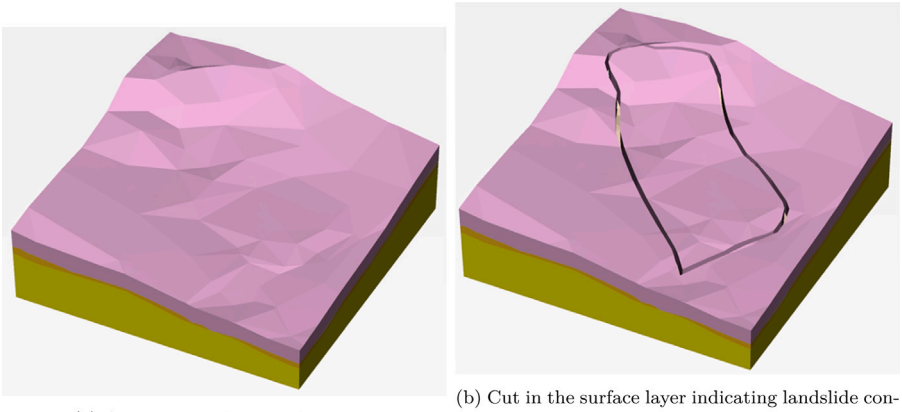

(a) Application of the surface layer

(b) Cut in the surface layer indicating landslide contour

Fig. 26. Steps in the application of the elastic surface layer.

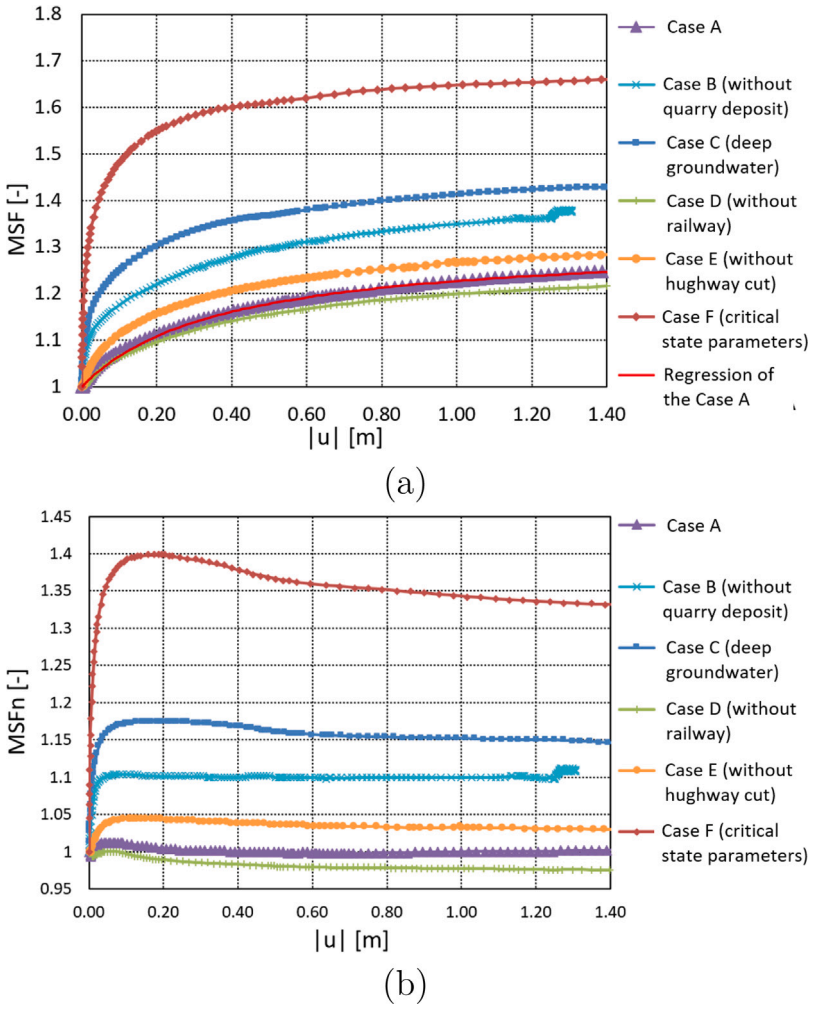

Fig. 27. Results of the stability analyses of Cases A-F in terms of MSF (a) and MSF_n (b) evolution. Displacements are measured at the surface in the centre of the landslide, MSF represents the strength reduction factor.

- Stability of Case A, which represents the actual slope geometry, groundwater level and residual strength parameters, resulted in a $FS = 1.227$. Attributing all the modelling uncertainties to the shear strength parameters of the failure zone allows us to estimate the residual friction angle acting in the shear zone, which would be $\varphi_r = \arctan(15°)/1.227 = 12.3°$. The fact that the failure was driven by the residual parameters and not by critical strength is also supported by Case F, which indicated a high stability factor $FS = 1.649$. Such a slope would be unlikely to fail.
- Stability analyses for cases other than case A (possibly with the exception of case D) demonstrate the effect of individual aspects and do not represent the actual failure potential of the slope. This is because, as clarified in later studies (Stemberk et al., 2019), the Dobkovičky landslide most likely developed retrogressively

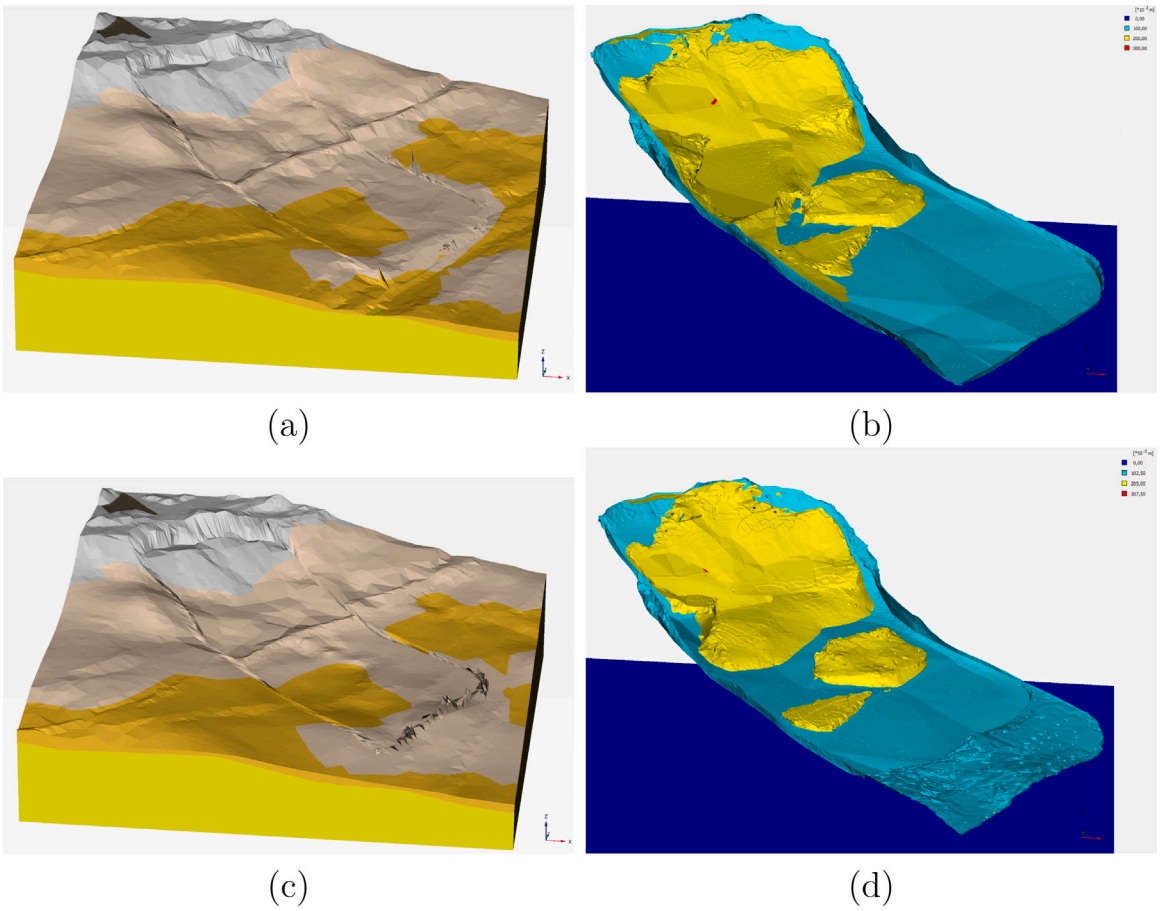

Fig. 28. Deformed mesh (a, c) and displacement contours (b, d) for case A (a, b) and case E (without highway) (c, d).

from the highway cut uphill during the three years preceding the landslide, after an exceptionally rainy period in 2010, with the gradual development of residual shear strength along the retrogressively developed failure zone. Therefore, analyses based on residual shear strength indicating a factor of safety higher than one are not representative of a potential failure scenario, since the residual strength used in the analyses is not likely to have developed. This is, in particular, the case of the analysis E (without highway cut).

- Cases B (without quarry deposits) and E (without the highway cut) both lead to factors of safety higher than 1, indicating that both the highway cut and quarry deposits contributed to the slope failure. As explained above, however, the highway cut had an additional major effect, being the likely starting point for the slip zone propagation. Also, when comparing the calculated values of the *FS*, it must be recalled that the actual landslide contour was different for case E since the calculated landslide was shorter than the real one.
- The case C (deep groundwater) shows that the groundwater level played a key role in the stability of the slope.
- The case D indicates that the railway embankment had a negligible effect on slope stability through its mechanical action. As revealed in Stemberk et al. (2019), however, it could have an additional affect on stability by supplying water into the slope through insufficiently maintained drainage along the embankment.

5. Conclusion

The paper introduced a method to calculate the factor of safety of complicated slopes, in particular in 3D, where the standard strength reduction applied within the finite element framework cannot be used because it stops calculating due to local instabilities. The method consist of applying a weightless elastic surface layer, which stabilizes the surface of the numerical model and thus prevents local failures. The method can be used to induce failures in the desired shape and location controlled, by defining their surface contours. The parametric study showed that the method is sensitive to cut width, which should be restricted to one or two finite elements to prevent local failures within the cut. The use of the surface layer method was subsequently demonstrated by means of back analysis of the Dobkovičky landslide in the Czech Republic. The effects of individual slope features (such as a highway cut and quarry deposits) were identified, which would not have been possible without application of the surface layer method.

CRediT authorship contribution statement

Tomáš Kadlíček: Conceptualization, Methodology, Validation, Formal analysis, Investigation, Data curation, Writing – original draft, Writing – review & editing Visualization, Project administration, . **David Mašín:** Conceptualization, Methodology, Validation, Formal analysis, Investigation, Resources, Data curation, Writing – original draft, Writing – review & editing Visualization, Supervision, Project administration, Funding acquisition.

Declaration of competing interest

Authors proclaim that they are not in a relationship with any organisation or group of people that can inappropriately influence their bias.

Data availability

Data will be made available on request

Acknowledgements

The first and second author acknowledge financial support from the research grant GACR 22-12178S. The second author acknowledges financial support from the research grant TACR CK02000203 and institutional support by the Center for Geosphere Dynamics (UNCE/SCI/006).

References

Bishop, A.W., 1954. The use of the slip circle in the stability analysis of slopes. Géotechnique 5, 7–17. http://dx.doi.org/10.1680/GEOT.1955.5.1.7.

Borges, L., Zouain, N., Costa, C., Feijóo, R., 2001. Adaptive approach to limit analysis. Int. J. Solids Struct. 38, 1707–1720. http://dx.doi.org/10.1016/S0020-7683(00)00131-1.

Bottero, A., Negre, R., Pastor, J., Turgeman, S., 1980. Finite element method and limit analysis theory for soil mechanics problems. Comput. Methods Appl. Mech. Engrg. 22, 131–149. http://dx.doi.org/10.1016/0045-7825(80)90055-9.

Camargo, J., Velloso, R.Q., Vargas, E.A., 2016. Numerical limit analysis of three-dimensional slope stability problems in catchment areas. Acta Geotech. 11, 1369–1383. http://dx.doi.org/10.1007/S11440-016-0459-3.

Carrara, A., Cardinali, M., Detti, R., Guzzetti, F., Pasqui, V., Reichenbach, P., 1991. GIS techniques and statistical models in evaluating landslide hazard. Earth Surface Processes and Landforms 16, 427–445. http://dx.doi.org/10.1002/ESP.3290160505.

Chen, Z., Mi, H., Zhang, F., Wang, X., 2011. A simplified method for 3D slope stability analysis. Can. Geotech. J. 40, 675–683. http://dx.doi.org/10.1139/T03-002.

Chen, X., Wang, D., Yu, Y., Lyu, Y., 2020. A modified Davis approach for geotechnical stability analysis involving non-associated soil plasticity. Geotechnique 70, 1109–1119. http://dx.doi.org/10.1680/JGEOT.18.P.158.

Chen, J., Yin, J.H., Lee, C.F., 2005. A three-dimensional upper-bound approach to slope stability analysis based on RFEM. Geotechnique 55, 549–556. http://dx.doi.org/10.1680/GEOT.2005.55.7.549.

Cheng, Y.M., Lansivaara, T., Wei, W.B., 2007. Two-dimensional slope stability analysis by limit equilibrium and strength reduction methods. Comput. Geotech. 34, 137–150. http://dx.doi.org/10.1016/J.COMPGEO.2006.10.011.

Chugh, A.K., 2003. On the boundary conditions in slope stability analysis. Int. J. Numer. Anal. Methods Geomech. 27, 905–926. http://dx.doi.org/10.1002/NAG.305.

Davis, E., 1968. Theories of plasticity and failures of soil masses. In: Soil Mechanics, Selected Topics. Butterwoth.

Duncan, J.M., 1996. State of the art: Limit equilmrium and finite element analysis of slopes. J. Geotech. Eng. 122, 577–596.

Fredlund, D.G., Scoular, R.E.G., Zakerzadeh, N., 1999. Using a finite element stress analysis to compute the factor of safety. In: 52nd Canadian Geotechnical Conf. pp. 73–80.

Gens, A., Hutchinson, J.N., Cavounidis, S., 1988. Three-dimensional analysis of slides in cohesive soils. Géotechnique 38, 1–23. http://dx.doi.org/10.1680/GEOT.1988.38.1.1.

Griffiths, D.V., Lane, P.A., 1999. Slope stability analysis by finite elements. Géotechnique 49, 387–403. http://dx.doi.org/10.1680/GEOT.1999.49.3.387.

Griffiths, D.V., Marquez, R.M., 2007. Three-dimensional slope stability analysis by elasto-plastic finite elements. Geotechnique 57, 537–546. http://dx.doi.org/10.1680/GEOT.2007.57.6.537.

Huang, C.C., Tsai, C.C., 2000. New method for 3D and asymmetrical slope stability analysis. J. Geotech. Geoenviron. Eng. Vol. 126, 917–927. http://dx.doi.org/10.1061/(ASCE)1090-0241(2000)126:10(917).

Huang, C.C., Tsai, C.C., Chen, Y.H., 2002. Generalized method for three-dimensional slope stability analysis. J. Geotech. Geoenviron. Eng. Vol. 128, 836–848. http://dx.doi.org/10.1061/(ASCE)1090-0241(2002)128:10(836).

Hungr, O., 2015. An extension of Bishop's simplified method of slope stability analysis to three dimensions. Géotechnique 37, 113–117. http://dx.doi.org/10.1680/GEOT.1987.37.1.113.

Janbu, N., 1954. Application of composite slip surface for stability analysis. In: Proceedings of the European Conference on Stability of Earth Slopes, Vol. 3. pp. 43–49.

Janbu, N., 1973. Slope Stability Computations. Wiley (John) and Sons.

Jia, N., Mitani, Y., Xie, M., Djamaluddin, I., 2012. Shallow landslide hazard assessment using a three-dimensional deterministic model in a mountainous area. Comput. Geotech. 45, 1–10. http://dx.doi.org/10.1016/J.COMPGEO.2012.04.007.

Kadlíček, T., Mašín, D., 2020. The strength reduction method in clay hypoplasticity. Comput. Geotech. 126, http://dx.doi.org/10.1016/j.compgeo.2020.103687.

Krahn, J., 2011. The 2001 R.M. Hardy lecture: The limits of limit equilibrium analyses. Can. Geotech. J. 40, 643–660. http://dx.doi.org/10.1139/T03-024.

Leshchinsky, D., Baker, R., 1986. Three-dimensional slope stability: End effects. Soils Found. 26, 98–110. http://dx.doi.org/10.3208/SANDF1972.26.4_98.

Li, A.J., Merifield, R.S., Lyamin, A.V., 2009. Limit analysis solutions for three dimensional undrained slopes. Comput. Geotech. 36, 1330–1351. http://dx.doi.org/10.1016/J.COMPGEO.2009.06.002.

Lin, H.D., Wang, W.C., Li, A.J., 2020. Investigation of dilatancy angle effects on slope stability using the 3D finite element method strength reduction technique. Comput. Geotech. 118, 103295. http://dx.doi.org/10.1016/J.COMPGEO.2019.103295.

Liu, S.Y., Shao, L.T., Li, H.J., 2015. Slope stability analysis using the limit equilibrium method and two finite element methods. Comput. Geotech. 63, 291–298. http://dx.doi.org/10.1016/J.COMPGEO.2014.10.008.

Lyamin, A.V., Sloan, S.W., 2002a. Lower bound limit analysis using non-linear programming. Internat. J. Numer. Methods Engrg. 55, 573–611. http://dx.doi.org/10.1002/nme.511.

Lyamin, A.V., Sloan, S.W., 2002b. Upper bound limit analysis using linear finite elements and non-linear programming. Int. J. Numer. Anal. Methods Geomech. 26, 181–216. http://dx.doi.org/10.1002/nag.198.

Lyamin, A.V., Sloan, S.W., Krabbenhøft, K., Hjiaj, M., 2005. Lower bound limit analysis with adaptive remeshing. Internat. J. Numer. Methods Engrg. 63, 1961–1974. http://dx.doi.org/10.1002/NME.1352.

Maier, G., Hueckel, T., 1979. Nonassociated and coupled flow rules of elastoplasticity for rock-like materials. Int. J. Rock Mech. Min. Sci. Geomech. Abstr. 16, 77–92. http://dx.doi.org/10.1016/0148-9062(79)91445-1.

Manzari, M.T., Nour, M.A., 2000. Significance of soil dilatancy in slope stability analysis. J. Geotech. Geoenviron. Eng. 126, 75–80. http://dx.doi.org/10.1061/(ASCE)1090-0241(2000)126:1(75).

Matsui, T., San, K.C., 1992. Finite element slope stability analysis by shear strength reduction technique. Soils Found. 32, 59–70. http://dx.doi.org/10.3208/SANDF1972.32.59.

Michalowski, R.L., Drescher, A., 2009. Three-dimensional stability of slopes and excavations. Géotechnique 59, 839–850. http://dx.doi.org/10.1680/GEOT.8.P.136.

Michalowski, R.L., Nadukuru, S.S., 2013. Three-dimensional limit analysis of slopes with pore pressure. J. Geotech. Geoenviron. Eng. 139, 1604–1610. http://dx.doi.org/10.1061/(ASCE)GT.1943-5606.0000867.

Morgenstern, N.R., Price, V.E., 1965. The analysis of the stability of general slip surfaces. Géotechnique 15, 79–93. http://dx.doi.org/10.1680/GEOT.1965.15.1.79.

Nian, T.K., Huang, R.Q., Wan, S.S., Chen, G.Q., 2012. Three-dimensional strength-reduction finite element analysis of slopes: Geometric effects. Can. Geotech. J. 49, 574–588. http://dx.doi.org/10.1139/T2012-014.

Nitzsche, K., Herle, I., 2020. Strain-dependent slope stability. Acta Geotech. 15, 3111–3119. http://dx.doi.org/10.1007/S11440-020-00971-3.

Peraire, J., Vahdati, M., Morgan, K., Zienkiewicz, O.C., 1987. Adaptive remeshing for compressible flow computations. J. Comput. Phys. 72, 449–466. http://dx.doi.org/10.1016/0021-9991(87)90093-3.

Petterson, K.E., 1955. The early history of circular sliding surfaces. Géotechnique 5, 275–296. http://dx.doi.org/10.1680/GEOT.1955.5.4.275.

Rudnicki, J.W., Rice, J.R., 1975. Conditions for the localization of deformation in pressure-sensitive dilatant materials. J. Mech. Phys. Solids 23, 371–394. http://dx.doi.org/10.1016/0022-5096(75)90001-0.

Sarma, S.K., 1979. Stability analysis of embankments and slopes. J. Geotech. Eng. Div. ASCE 105, 1511–1524. http://dx.doi.org/10.1061/ajgeb6.0000903.

Schneider-Muntau, B., Medicus, G., Fellin, W., 2018. Strength reduction method in Barodesy. Comput. Geotech. 95, 57–67. http://dx.doi.org/10.1016/j.compgeo.2017.09.010.

Šejnoha, M., 2015. Finite Element Analysis in Geotechnical Design. Saxe-Coburg Publications, Kippen, Stirling, Scotland.

Sloan, S.W., 1988. Lower bound limit analysis using finite elements and linear programming. Int. J. Numer. Anal. Methods Geomech. 12, 61–77. http://dx.doi.org/10.1002/NAG.1610120105.

Sloan, S.W., 1989. Upper bound limit analysis using finite elements and linear programming. Int. J. Numer. Anal. Methods Geomech. 13, 263–282. http://dx.doi.org/10.1002/NAG.1610130304.

Spencer, E., 1967. A method of analysis of the stability of embankments assuming parallel inter-slice forces. Géotechnique 17, 11–26. http://dx.doi.org/10.1680/GEOT.1967.17.1.11.

Stemberk, J., Mašín, D., Balek, J., Blahůt, J., Hartvich, F., Chaloupka, D., Kadlečík, P., Kalinová, R., Klimeš, J., Král, J., Kusák, M., Rott, J., Rybář, J., Špaček, P., Tábořík, P., 2016. Analysis of the D8 Highway Landlide by Dobkovičky Village (in Czech). Technical Report, Institute of Rock Structure and Mechanics, Czech Academy of Sciences, Available from https://www.mdcr.cz/Dokumenty/Silnicni-doprava/Pozemni-komunikace/Analyza-pricin-vzniku-sesuvu-na-dalnici-D8-u-Dobko.

Stemberk, J., Mašín, D., Král, J., Rott, J., Chaloupka, D., Hartvich, F., Klimeš, J., Tábořík, P., 2019. Revision Expert Opinion No. 22 – 4/2019 in the Matter of the Assessment of the Causes of the Landslide on the Construction of the D8 0805 Highway. Technical Report, Institute of Rock Structure and Mechanics, Czech Academy of Sciences.

Stianson, J.R., Chan, D., Fredlund, D.G., 2015. Role of admissibility criteria in limit equilibrium slope stability methods based on finite element stresses. Comput. Geotech. 66, 113–125. http://dx.doi.org/10.1016/J.COMPGEO.2015.01.014.

Stianson, J.R., Fredlund, D.G., Chan, D., 2011. Three-dimensional slope stability based on stresses from a stress-deformation analysis. Can. Geotech. J. 48, 891–904. http://dx.doi.org/10.1139/T11-006.

Taylor, D.W., 1937. Stability of earth slopes. J. Boston Soc. Civ. Eng. 24 (3), 197–247.

Tschuchnigg, F., Schweiger, H.F., Sloan, S.W., 2015a. Slope stability analysis by means of finite element limit analysis and finite element strength reduction techniques. Part I: Numerical studies considering non-associated plasticity. Comput. Geotech. 70, 169–177. http://dx.doi.org/10.1016/j.compgeo.2015.06.018.

Tschuchnigg, F., Schweiger, H.F., Sloan, S.W., 2015b. Slope stability analysis by means of finite element limit analysis and finite element strength reduction techniques. Part II: Back analyses of a case history. Comput. Geotech. 70, 178–189. http://dx.doi.org/10.1016/j.compgeo.2015.07.019.

Tschuchnigg, F., Schweiger, H.F., Sloan, S.W., Lyamin, A.V., Raissakis, I., 2015c. Comparison of finite-element limit analysis and strength reduction techniques. Geotechnique 65, 249–257. http://dx.doi.org/10.1680/geot.14.P.022.

Tu, Y., Liu, X., Zhong, Z., Li, Y., 2016. New criteria for defining slope failure using the strength reduction method. Eng. Geol. 212, 63–71. http://dx.doi.org/10.1016/J.ENGGEO.2016.08.002.

Ugai, K., 1985. Three-dimensional stability analysis of vertical cohesive slopes. Soils Found. 25, 41–48. http://dx.doi.org/10.3208/SANDF1972.25.3_41.

Wang, D., Chen, X., Yu, Y., Jie, Y., Lyu, Y., 2019a. Stability and deformation analysis for geotechnical problems with nonassociated plasticity based on second-order cone programming. Int. J. Geomech. 19, 04018190. http://dx.doi.org/10.1061/(ASCE)GM.1943-5622.0001339.

Wang, L., Sun, D., Li, L., 2019b. Three-dimensional stability of compound slope using limit analysis method. Can. Geotech. J. 56, 116–125. http://dx.doi.org/10.1139/CGJ-2017-0345.

Wei, W.B., Cheng, Y.M., Li, L., 2009. Three-dimensional slope failure analysis by the strength reduction and limit equilibrium methods. Comput. Geotech. 36, 70–80. http://dx.doi.org/10.1016/J.COMPGEO.2008.03.003.

Xie, M., Esaki, T., Cai, M., 2006a. GIS-based implementation of three-dimensional limit equilibrium approach of slope stability. J. Geotech. Geoenviron. Eng. 132, 656–660. http://dx.doi.org/10.1061/(ASCE)1090-0241(2006)132:5(656).

Xie, M., Esaki, T., Qiu, C., Wang, C., 2006b. Geographical information system-based computational implementation and application of spatial three-dimensional slope stability analysis. Comput. Geotech. 33, 260–274. http://dx.doi.org/10.1016/J.COMPGEO.2006.07.003.

Xie, M., Esaki, T., Zhou, G., Mitani, Y., 2003. Geographic information systems-based three-dimensional critical slope stability analysis and landslide hazard assessment 1. J. Geotech. Geoenvironmental Eng. 129, 1109–1118. http://dx.doi.org/10.1061/ASCE1090-02412003129:121109.

Yang, Y., Liu, F., Wu, W., 2022. Assessing slope stability with an improved 3D numerical manifold method. Rock Mech. Rock Eng. 55 (10), 6409–6423.

Yang, X.L., Wei, J.J., 2021. Analytical approach for stability of 3D two-stage slope in non-uniform and unsaturated soils. Eng. Geol. 292, 106243. http://dx.doi.org/10.1016/J.ENGGEO.2021.106243.

Yang, Y., Wu, W., Zheng, H., 2023. Investigation of slope stability based on strength-reduction-based numerical manifold method and generalized plastic strain. Int. J. Rock Mech. Min. Sci. 164, 105358.

Yang, Y., Xia, Y., Zheng, H., Liu, Z., 2021. Investigation of rock slope stability using a 3D nonlinear strength-reduction numerical manifold method. Eng. Geol. 292, 106285.

Zhang, T., Cai, Q., Han, L., Shu, J., Zhou, W., 2017. 3D stability analysis method of concave slope based on the Bishop method. Int. J. Mining Sci. Technol. 27, 365–370. http://dx.doi.org/10.1016/J.IJMST.2017.01.020.

Zheng, H., 2012. A three-dimensional rigorous method for stability analysis of landslides. Eng. Geol. 145–146, 30–40. http://dx.doi.org/10.1016/J.ENGGEO.2012.06.010.

Zheng, H., Liu, D.F., Li, C.G., 2005. Slope stability analysis based on elasto-plastic finite element method. Internat. J. Numer. Methods Engrg. 64, 1871–1888. http://dx.doi.org/10.1002/NME.1406.

Zhou, X.P., Cheng, H., 2013. Analysis of stability of three-dimensional slopes using the rigorous limit equilibrium method. Eng. Geol. 160, 21–33. http://dx.doi.org/10.1016/J.ENGGEO.2013.03.027.

Zienkiewicz, O.C., Huang, M., Pastor, M., 1995. Localization problems in plasticity using finite elements with adaptive remeshing. Int. J. Numer. Anal. Methods Geomech. 19, 127–148. http://dx.doi.org/10.1002/NAG.1610190205.

Zienkiewicz, C., Humpheson, C., Lewis, R.W., 1975. Associated and Non-Associated Visco-Plasticity and Plasticity in Soil Mechanics, Vol. 25. Technical Report, pp. 671–689.